University of Alberta

A molecular dynamics modeling study on the mechanical behavior of nano-twinned Cu and relevant issues

by

Lei Yue

A thesis submitted to the Faculty of Graduate Studies and Research

in partial fulfillment of the requirements for the degree of **Master of Science**

in

Materials Engineering

Department of Chemical and Materials Engineering

©Lei Yue

Fall 2010

Edmonton, Alberta

Examining Committee

Li, Dongyang Chemical and Materials Engineering

Zhang, Hao Chemical and Materials Engineering

Raboud, Donald Mechanical Engineering

Abstract

As a candidate for dynamic electric contacts, Nano-twinned copper has intrinsic conductivity and enhanced fretting resistance. To better understand its general mechanical behavior, we conduct molecular dynamics simulation studies to investigate responses of nano-twinned copper to stress and to one-directional and two-directional sliding processes, in comparison with single crystal and nano-grained model systems. Obtained results suggest that the twin boundary blocks dislocation movement more effectively and the degree of emitting dislocations under stress is considerably lower than that of grain boundary. The inverse H-P relation only occurring in nano-grained materials does not necessarily result from grain boundary sliding. Under sliding conditions, dislocations are easier to be generated in the single crystal system. During the two-directional sliding process, Bauschinger effect is observed in the single crystal and nano-twinned systems, while the situation is opposite for the nano-grained system. The nano-twinned Cu shows the least dislocation accumulation during two-directional sliding.

Acknowledgements

Table of Contents

List of Tables

List of Figures

used to reflect the local stress magnitude. (d), (e) and (f) illustrate the lattice distortion and spots of high stress concentrations in the three systems, respectively, where plastic deformation is likely initiated. 58

Figure 4.1 Three model systems: (a) Single crystal model system with crystal orientation $[111], [\bar{1}10]$ and $[11\bar{2}]$ in the X-, Y- and Z- directions (b) Twin boundary model system. The left grain has orientations $[111]$, $[\bar{1}10]$ and   in the X-, Y- and Z-directions. The right grain is tilted to the orientations.. 77

of $[111]$, $[1\bar{1}0]$ and $[\bar{1}\bar{1}2]$. (c) Grain boundary model system. The left grain has orientations $[111]$, $[\bar{1}10]$ and $[11\bar{2}]$ in the X-, Y- and Z-directions. The right grain is twisted to the orientations of $[111], [\bar{5}41]$ and $[12\bar{3}]$. 1% vacancies are added to the boundary region. A rigid indenter tip with its radius of 5nm as shown in the figure was used to investigate the response of the system to sliding wear. The tip has copper's

Chapter1 Introduction

Electrical contacts in dynamic systems made of conductive materials are required to be resistant to fretting while maintaining high electrical conductivity due to the fact that fretting results in loss of conductivity[1, 2], since generated dislocations increase the contact resistance, raise the interfacial temperature, and thus make the contacts dysfunctional. Figure 1.1 shows a damaged contact sample under fretting loading.
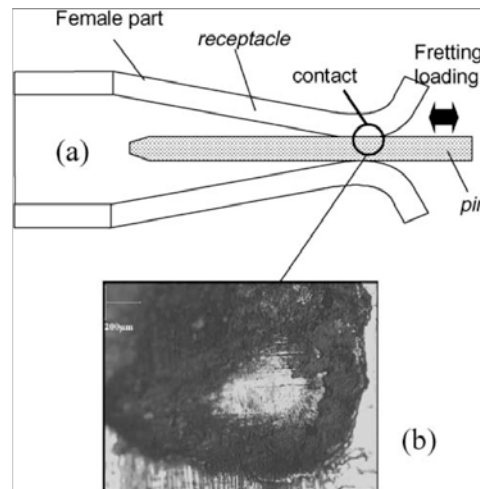
Figure 1.1 Fretting in connectors (a) Schematic representation of fretting work condition. (b) Observation of the fretting damage contact[1].

It was expected that nanocrystalline (NC) copper could be a candidate due to its considerably improved mechanical strength[3]. Indeed, compared to its microcrystalline counterpart, nanocrystalline copper possesses considerably enhanced wear resistance. However, nanocrystalline Cu shows

significantly deteriorated conductivity due to strong electron scattering at high-density grain boundaries. Recent experimental studies suggest that nano-sized twin boundaries (TW) in copper could be a solution to such a dilemma. It is reported that nano-twinning can act as nano-sized grain boundary (GB) and bring in ultra-high strength to copper with minimal influence on its conductivity. The minimal influence of twin boundaries on the conductivity is understandable, since twin boundaries structure is less disordered than grain boundaries[4-6]. The scattering of electrons by ordered twin boundaries is much smaller than that by grain boundaries. Regarding the mechanical behavior, grain boundaries act as both sink and source to attract and emit dislocations under stress[7, 8], resulting in certain variations in strength and ductility. Twin boundaries may play similar roles but relevant information is rather limited. In particular, there is lack of the information about the response of twin boundaries to stress at the nanoscale, at which dislocations have very limited free space or free path to move.

Dao et al[9] studied nanocrystalline copper with experimental focus on its mechanical properties. However, it is difficult to experimentally investigate the local response of twin boundaries to stress at nanoscale, although the overall mechanical behavior of copper containing nano-twin boundaries can be experimentally evaluated. In this regard, atomistic simulation is a useful tool to investigate material structures and corresponding mechanical properties at the nanoscale[10-13]. The computer simulation method is chosen as the researching method in this thesis. The response of twin

boundaries at the nanoscale to stress in comparison with grain boundaries in copper is studied using molecular dynamics method (MD) and the details of this method are discussed in Chapter 3.

It is known that the relation between the grain size and the strength of nanocrystalline metals can be described by the Hall-Petch relationship (simplified as H-P). However, when the grain size is very small, the so-called inverse Hall-Petch relationship is observed in some NC metals[14, 15]. Grain boundary sliding and grain rotation[11, 16-18] are considered as reasons for materials softening. However, lacking solid experimental evidence or sound theoretical analysis, the mechanism responsible for the transition from H-P relation to inverse H-P is still not well understood. In this study, we simulate deformation processes of three systems, including single crystal, one crystal with two twin boundaries, and one with two grain boundaries, with different grain sizes in order to see whether there is a change from H-P relationship to an inverse H-P one in the copper systems. We simply focus on the local responses of nano-twinned and nano-grained systems to external stress in the critical size range of nano-crystals. What's more, the tensile tests are performed under uniaxial loading and the edges of sample at tensile direction are fixed. In such a case, the grain boundary sliding unlikely occurs, so that we could examine whether the inverse H-P relationship exists without sliding occurring at boundaries.

Electrical contacts in dynamic systems suffer from fretting in the contract area, which introduces plastic deformation and raises temperature, both of

which increase the electrical contact resistance by enhanced electron scattering by defects such as dislocations and possible oxidation. During fretting, plastic deformation is accumulated, which increases the electrical resistance. It is noticed that the responses of a metal to different wearing conditions, i.e., one-directional wear and two-directional wear (back-and-forth) are very different. In the latter case, material softening could occur while hardening always occurs during one-directional sliding. Thus one of our objectives of this thesis study is to investigate the dislocation accumulation in single crystal, twin boundary and grain boundary copper systems, and get an insight into the behavior of the materials during one-directional and two-directional sliding wear processes.

This thesis has the following structure; background and motivations of this thesis are introduced in the first chapter. Relevant information on the twin boundary structure, history of nanotwinning discovered in face-centered cubic (FCC) metals, experimental and simulations related to nano-twinned structure mechanical properties are provided as a literature review. In chapter 2, the computational techniques for characterizing atomic motions, molecular dynamics simulation details such as selected inter-atomic potentials, temperature and pressure control, order parameter used for recognizing localized crystal structure, principal stress calculations are described and discussed. In Chapter 3, simulation studies on responses of three different model systems, single crystal, twin boundary and grain boundary in nanocrystalline copper, to stress at the nanoscale with range of

5 ~ 25 nm are reported. In Chapter 4, MD simulation studies on how the nano-twinning affects the increase in the local dislocation density, in comparison with nano-GBs under one-directional and two-directional sliding conditions are reported. In Chapter 5, a summary of the present studies is given and directions for future work in this area and remaining questions will also be discussed.

1.1 Twin boundary definition

Twin boundary is a special grain boundary, which is a highly symmetrical interface. Atoms belonged to twin boundary are shared by the two crystals, with one of the crystal the mirror image of the other. Compared to general grain boundary, the perfect twin boundary has ordered structure and low boundary energy. A definition is given: A twin is a region of a crystal in which the orientation of the lattice is a mirror image of that in the rest of the crystal[19]. Figure 1.2 illustrates deformation twining found in alumina[20]. With red line marked, a mirror symmetric structure is observed of the twin band.
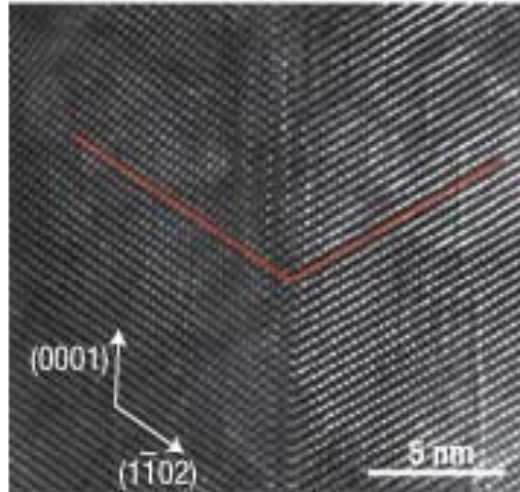
Figure 1.2 High resolution electron microscopy image of deformation twins in alumina fragments. The red lines show the mirror symmetry of the twin band with the matrix[20].

In order to describe a twin, a twin notation system is used (see Figure 1.3). This sphere shows a part of material and the top half material is sheared on K_1 plane along the direction of shear η_1 forming a twinning. K_1 is called the twinning plane. After sheared, plane K_2 remained undistorted. The second characteristic direction η_2 lies in K_2 and perpendicular to the intersection of K_1 and K_2. (Original position is plane K_2' and η_2') With these twin elements, we could define twins in different crystal structures. For example, in FCC crystals, twinning occurs on $K_1 = \{111\}$ planes $\eta_1 = <11\overline{2}>$ direction and $K_2 = \{11\overline{1}\}$ and $\eta_2 = <112>$. Figure 1.4 illustrates the atomic movement in FCC crystal in $\{111\}<11\overline{2}>$ twinning.
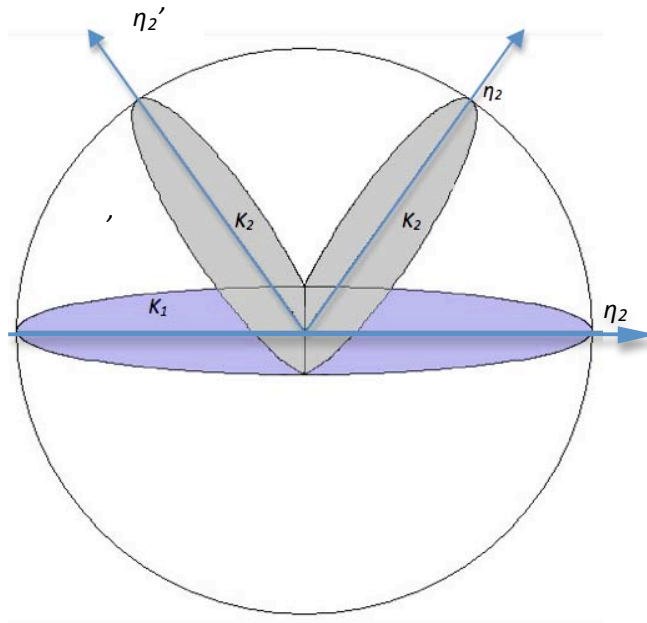
Figure 1.3 Twin notation system. The two undistorted planes are K_1 and K_2.

The shear direction is η_1. The second characteristic direction is η_2.
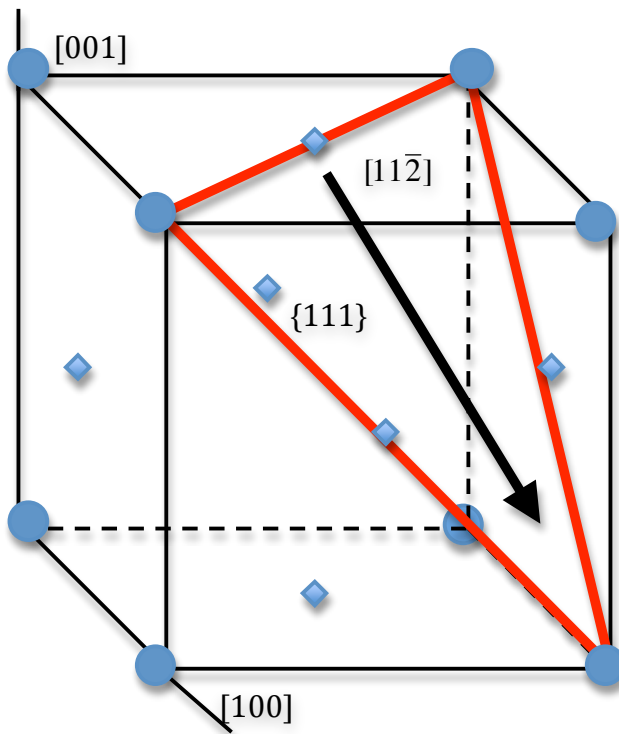
Figure 1.4 Atomic displacement in $\{111\}<11\bar{2}>$ twinning of FCC metals.

$\{111\}$ is the twin plane, $<11\bar{2}>$ is the shear direction.

1.2 Deformation twinning in FCC materials

It was believed for many years that a FCC metal does not deform by twinning, since it has enough slip systems to fulfill the deformation. However, in 1957, Blewitt, Coltman and Redman [21] performed tensile tests on single crystal of copper at low temperatures, 4.2K and 77.3K. During these experiments, mechanical twinning has been observed for the first time in FCC metals using X-ray method. After this initial work, additional observations of such twinning in FCC materials have been reported. In 1964, Nolder and Thomas[22] showed microtwinning in nickel when sample was shock loaded at 350 kb and higher. The same year, Johari and Thomas [23] reported that in explosively deformed copper, the mode of deformation could change from slip to microtwinning due to stacking fault energy differences.

After observed in copper and nickel, for a period of time, no experiments showed deformation twins existed in single or polycrystalline pure aluminum. Suggested by molecular dynamics simulation[24], deformation twinning has been observed experimentally in nanocrystalline aluminum [25] by Chen et al in 2003, see Figure 1.5. When grain size decreases to the nanoscale, the deformation mechanisms transit from normal slip to partial dislocation initiation. Thus deformation twinning was observed in samples with small grain size.
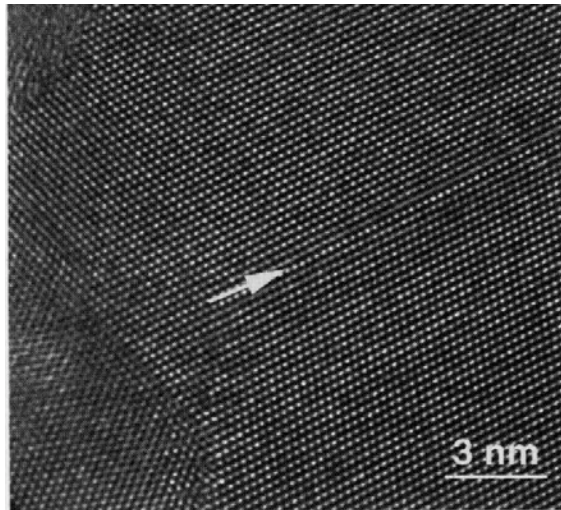
Figure 1.5 High resolution electron microscopy image of growth twin boundary in grain size from 10 to 35nm. The white arrow marks a Σ3{111} twin boundary[25].

1.3 Ultrahigh strength in nano-twinned Cu

It was reported that nanocrystalline metals with grain sizes less than 100nm have strengths exceeding those of coarse-grained and even alloyed metals[26]. But with improving the strength, nanocrystalline materials often exhibit low tensile ductility, which leads to a limit in use.

To solve this problem, Wang et al[3] studied a thermomechanical treatment of Cu by rolling the copper sample in liquid nitrogen with a high value of percentage cold work. Such low temperature treatment allows a number of dislocations accumulated inside grains at a steady state, even stable at room temperature. Thus the resulting material has a typical heavily deformed microstructure with high densities of dislocations, high tensile

strength and high ductility. To achieve such superior mechanical properties, there are three factors. First, the thermomechanical treatment allows an inhomogeneous microstructure to form. As shown in Figure 1.6 (b), the nanocrystalline sized grains take most area of the sample, while small amount of large grains are embedded among them. Treated by cold work, the deformation grains are under multi-axial stress state. Such complex stress state and complicated dislocation configurations are beneficial for dislocation storage. Second, when the overall uniform elongation reaches the maximum strain, larger grains accumulate large numbers of twin boundaries, dislocations and subgrain boundaries, which refines the microstructure to a nanocrystalline level. Such refinement is considered as an improvement of strain hardening. Third, unexpected twinning is observed inside grains, see Figure 1.6 (a). Since dislocations pileups at the twin boundaries, the existence of twinning is considered very effective in enhancing strain hardening. With three factors mention above, a good combination of strength and ductility is achieved.
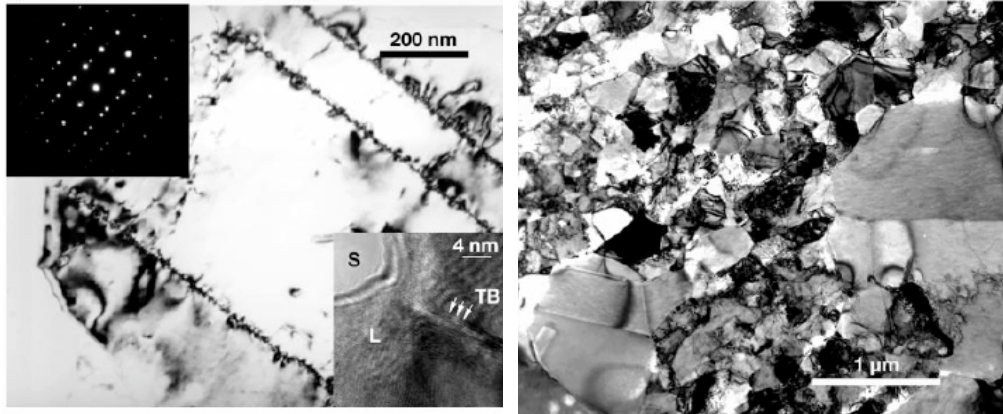
(a)   (b)

Figure 1.6 (a) Transmission electron micrograph of Cu after tensile strains The lower right inset shows a twin boundary is seen near the tip of the smaller ultrafine grain S protrusion into a larger, micrometer-sized grain L, where twinning is initiated. (b) The majority of the grains are in the nanocrystalline/ultrafine range, with some crystallized regions[3].

Compared to previous study of nanocrystalline materials, Wang's work had made an improvement of materials mechanical properties. The existence of nano-twinned structure is considered to play a role in combination of high strength and high ductility. However, the resulting material described above has an inhomogeneous structure, which contains grain boundaries, twin boundaries, nanocrystalline and crystallized grains. In this case, it is not easy to tell the contribution from nano-twinned structure to material's mechanical behavior. In order to study the details of nano-twinning effect, how to construct nano-twined model in nanocrystalline material becomes a research topic.

Lu's group succeeded in making high-purity Cu (>99.99%) sample with growth twins[6]. The samples are synthesized using a pulsed electrodeposition from a Cu_2SO_4 bath. The pulsed electrodeposition is carried out galvanostatically using cathodic square wave pulses by turning off the current periodically. The peak current density is 0.5 A/cm^2 and the pH value is about 1. A highly purified (99.99%) electrolytic copper sheet is used as the soluble anode without additional organic additive in the solutions. As shown in Figure 1.7 (A) the as-deposited Cu consists of irregular shaped grains with random orientations. The grain sizes are between 100nm and 1μm, with an average value of about 400nm. Each grain contains a high density of growth twins. Different twin thickness (spacing between adjacent twin boundaries, illustrated as Figure 1.7 (B)) can be achieved by adjusting the electrodeposition parameters. With the help of such nano-twinned structure sample, a series of experiments were explored to study its mechanical properties.
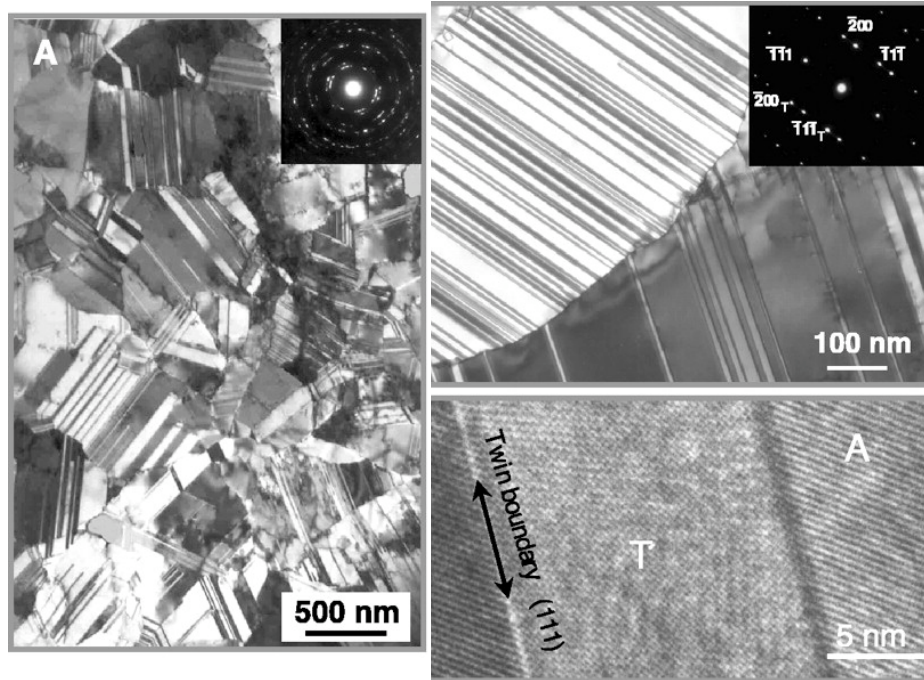
Figure 1.7 TEM image of microstructure in an as-deposited Cu sample (A) Submicrometer-sized grains with random orientation (B) Twins in each grain are parallel to each other (C) Closer look of twin boundary[6]

Tensile strength is an important mechanical parameter used for choosing electron conductor materials in industry. Ma et al[27] and Lu el al[6] performed tensile tests on nano-twinned copper (as-deposited Cu sample) compared with nanocrystalline and coarse grain Cu. The as-deposited samples are cut into dog-bone shaped specimens, see Figure 1.8, with a gauge length of 4 mm, a width of 2 mm and a thickness of 16-25 μm determined using scanning electron microscopy. The coarse grain samples are prepared by annealing the as-deposited Cu at 900°c for 10 hours. Nanocrystalline (nc) Cu is pure copper with three dimensional grain sizes down to nanoscale.

Uniaxial tensile tests are performed in a Tytron 250 Microforce Testing System (produced by MTS) at a strain rate of $6 \times 10^{-3} s^{-1}$. Transmission electron microscopy is performed on a JEM- 2000EXII electron microscopy operated at 200 kV. Results are presented as stress strain curve in Figure 1.8. The tensile yield stress of nano-twinned Cu reaches 900Mpa and ultimate tensile stress is 1068 MPa. These values are much higher than nanocrystalline and coarse-grained Cu. The yield stress of nano-twinned sample is about one order of magnitude larger than those of coarse-grained Cu sample. Besides, nano-twinned Cu shows a considerable tensile ductility, which is much larger than nanocrystalline Cu. Although nano-twinned structure does not naturally exist in FCC materials, with the help of high-tech manufacture method, nano-twinned microstructure could be produced to optimize materials with superior mechanical properties.
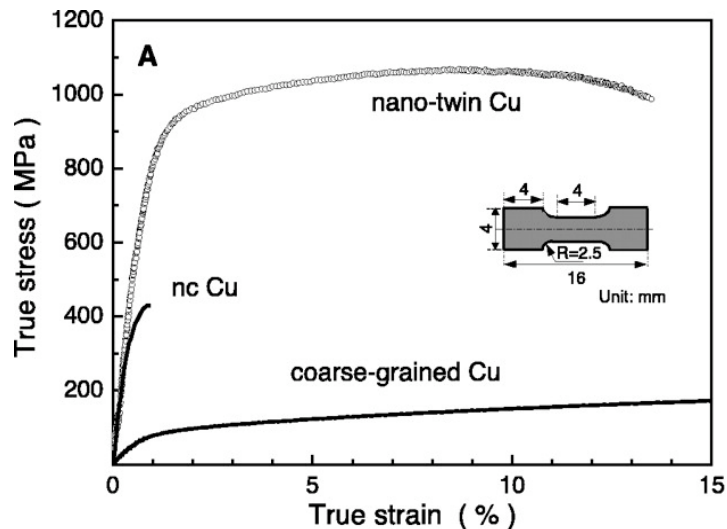
Figure 1.8 Tensile stress-strain curve for nano-twinned Cu compared with nanocrystalline Cu and coarse-grained polycrystalline Cu sample[6]

In order to study the origin of high strength behavior in nano-twinned Cu, close observations of twin boundaries are made using high resolution TEM[6]. The image, Figure 1.9, suggests that dislocations are located at twin boundaries, which implies that twins block the propagation of slip bands. Additionally, a series of samples with different twin densities are prepared and tested under tensile test. It is reported that with a decrease in the twin density, both tensile yield stress and ultimate stress drop[6, 28]. The reported results demonstrate that the twin boundary plays an important role in strengthening copper. The twin boundary behaves like general grain boundaries in acting as an obstacle to dislocation movement and performs more effectively. However, there are still unclarified issues. For example, does a twin boundary act as both a sink and a source of dislocations, similar to the grain boundary? How does the grain size of nano-twinned materials affect mechanical properties? More studies are clearly needed in order to understand and take advantage of nano-twinned materials.
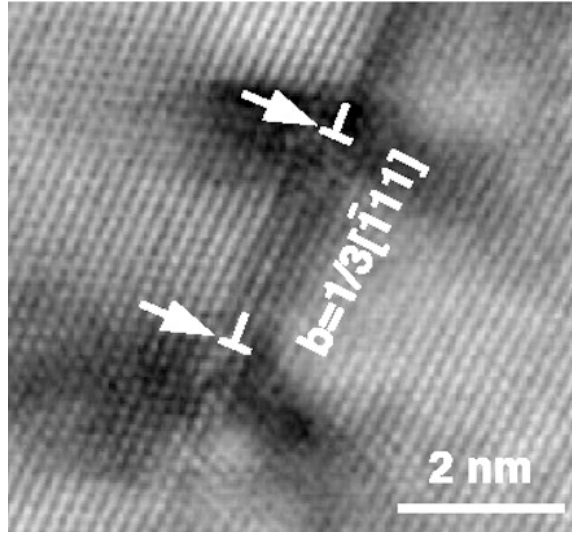
Figure 1.9 High resolution TEM image of twin boundary with Frank dislocations[6]

1.4 Softening in nanocrystalline Cu

It is known that variations in the grain size of materials result in changes in their mechanical behavior. The relation between the grain size and the strength of nanocrystalline metals can be described by the Hall-Petch relationship[29, 30]. Smaller grain size will make material harder. It obeys the Hall-Petch relationship. In industry, reduction of grain size through thermo mechanical possessing is based on such a mechanism. However, this proportional trend between strength and grain size is found reversed when the grain size decreased to a certain value, as described by the so-called inverse Hall-Petch relation. The inverse H-P relationship is usually ascribed to grain boundary sliding [31, 32]. Since twin boundary is considered as a special grain boundary, whether or not TW-containing material has such

behavior is unknown.

1.4.1 Hall-Petch relationship in nanocrystalline materials

The Hall-Petch[29, 30] relationship is used to describe the relation between yield stress σ_y and grain size. The classical Hall-Petch equation is shown

$$\sigma_y = \sigma_0 + \frac{k}{\sqrt{d}}$$
[1.4.1]

where σ_0 is approximately the yield stress of a very coarse-grained polycrystal, d is the grain size, and k is the material constant. As Eqn. [1.4.1] shows, the yield strength is inversely proportional to the square root of grain size d. With grain size decreases, the yield strength becomes higher. Obeyed Hall-Petch relationship, the nanocrystalline material will result in extremely high yield strengths due to its small grain size. However, this is not observed and experiment results[14, 15, 26] suggest that, below a certain constant grain size, the Hall-Petch relation start to break down. The yield strength becomes lower as the grain size decreases, leading to the inverse Hall-Petch relationship.

The inverse H-P relationship for NC metals is usually ascribed to grain boundary sliding. Atomistic simulations[31-35] have shown that the main deformation at grain boundaries may consist of localized sliding accompanied by some accommodation mechanism that maintains the intergrain compatibility. Results of recent atomistic simulation have shown

the crossover from the direct to the inverse grain-size dependency of the material strength[11]. Regardless of the theoretical studies, there is no solid and direct experimental conformation for these possible mechanisms as mentioned earlier. In a nanocrystalline metal, a large number of the triple-points of grain boundaries may make the GB sliding less easy at room temperature. Thus, the mechanism responsible for the transition from Hall-Petch relation to inverse Hall-Petch one as the grain size decreases to a certain level is still not well understood, lacking solid experimental evidence or sound theoretical analysis.

1.4.2 Hall-Petch relationship in nano-twinned Cu

Lu et al reported the inverse relationship also existed in nano-twinned Cu system[28]. As introduced in chapter 1.3, with controlling the deposition rate samples, twin boundaries with different spacing could be produced. In the reported study[28], a series of samples with different twin boundary thickness, ranging from 4 nm to 100nm, are prepared for tensile tests. The spacing between two adjacent twin boundaries (twin boundary thickness) may be defined as the twin "grain" size. Corresponding stress-strain curves are shown in Figure 1.10; nano twin (nt) 15 means that the spacing between two adjacent twin boundaries is 15nm. Stress-strain curve of a Coarse-grained Cu is presented as a reference (marked by cg). It is demonstrated that the nano-twinned Cu has considerably higher strength

than coarse-grained Cu. As twin thickness decrease from 100nm to 15nm, the yield stress continues increasing, which followed the Hall-Petch relationship. When thickness reaches 15nm, the peak value of nano-twined yield stress is achieved. As twin grain size keeps decreasing, the yield stress starts to decrease, which illustrates a softening phenomenon.
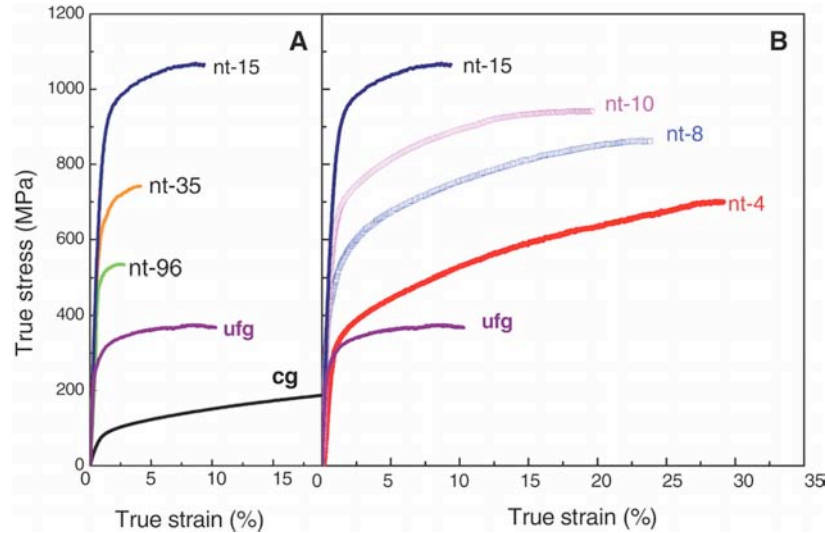
Figure 1.10 True stress-true strain curve for nt-Cu (A) Curves for samples with mean twin thickness varying from 15 to 96nm (B) Curves for samples with mean twin thickness varying from 4 to 15 nm. Ultrafine-grained (ufg) Cu with a mean grain size of 500nm and a coarse-grain (cg) Cu with a mean grain size of 10 μm are included for comparison[28].

Twin boundary behaves as a barrier blocking dislocations movement, a decrease in the thickness of twinning zone or an increase in the number of twin boundaries, in a unit volume, dislocations are blocked more frequently. As a result, the yield stress or strength increases. When the thickness of

twinning zone decreases from 10 to 4nm, since twin boundaries are different from grain boundaries, whether the softening may occur or the inverse Hall-Petch relation may exist is a question. In the nano-twinned Cu samples as reported[28], dislocation arrays at grain boundaries and partial dislocations along twin boundaries can be potential dislocation sources, which are expected to affect the initiation of plastic deformation. Thus, the contribution of twin boundary to this yielding process cannot be demonstrated experimentally. In this case, computer simulation could be a useful approach to have a look at this situation.

1.5 Electrical resistance of nanocrystalline Cu

It is discussed in previous sections that nanocrystalline Cu has a higher strength than coarse gained Cu. High strength is beneficial to the wear resistance. However, electrical contacts are also required to have low electrical resistance or high electrical conductivity. Nanocrystalline Cu with high density grain boundaries cannot sustain the electrical conductivity at the level of its coarse-grained counterpart due enhanced electron scattering.

Qian et al[36] studied the electrical resistivity of nano Cu with its grain boundaries in a fully relaxed state. The mean grain size of samples under study varies from 19 to 22nm. A sample having its grain size equal to 350nm (coarse-grained sample) is used as a reference sample. Figure 1.11 illustrates the relationship between grain size and electrical resistivity at different

temperatures. Clearly, nanocrystalline Cu has considerably larger electrical resistance, compared to that of the coarse-grained sample. As shown, as the grain size decreases, the electrical conductivity deteriorates. The disordered structure of grain boundaries disturbs the channels or paths for electrons to migrate, thus leading to higher electrical resistivity. Such an increase in electrical resistivity is significantly amplified by nanocrystallization. Therefore, nanocrystalline Cu is not a solution for electrical contacts requiring both high electrical conductivity and high wear/fretting resistance for dynamic systems.

Fig. 2. The temperature dependence of electrical resistivity (ρ) of samples A–E at a temperature range of 16–290 K.
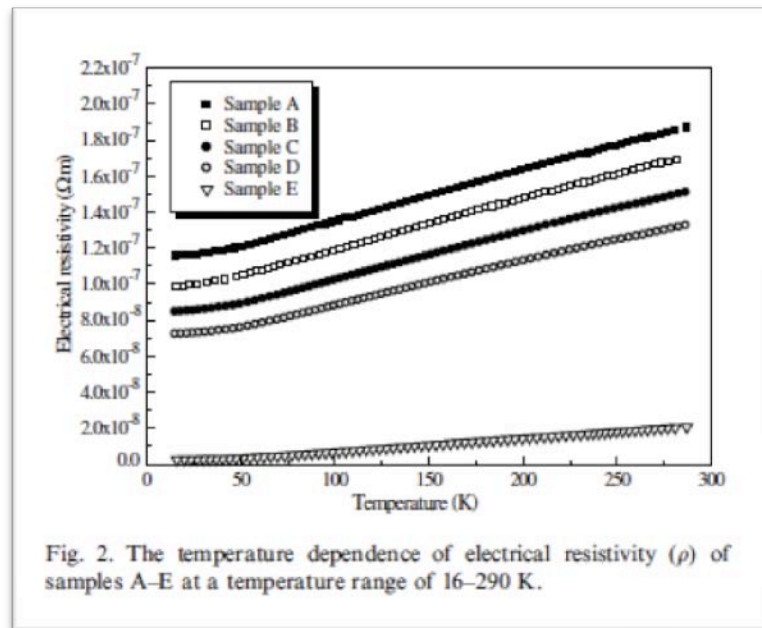
Figure 1.11 The temperature dependence of electrical resistivity of different grain-sized nanocrystalline Cu (Sample A has a grain size of 19nm, Sample B is 21 nm, Sample C is 22 nm, Sample D is 22 nm, Sample E is 350 nm)[36]

1.5.1 High electrical conductivity of nano-twinned Cu

Although nanocrystalline Cu exhibits high strength, its large electrical resistance prevent it from being a good candidate for electrical contacts in dynamics systems. Nano-twinned Cu has shown great promise for such applications. Lu et al [6] studied the electrical resistivity of as-deposited nano-twinned Cu and compared it with that of nanocrystalline copper and coarse-grained copper. As shown in Figure 1.12, nano-twinned Cu has slightly higher electrical resistance than coarse-grained Cu, while nanocrystalline Cu shows significantly larger electrical resistance in the entire range of temperatures under study. Compared to nanocrystalline Cu, nano-twinned Cu has relatively ordered structure, which generates less electron scattering[37, 38] than impurities and defects in grain boundary structure[5]. Superior mechanical properties and low electrical resistance make nano-twinned Cu a good candidate for electrical conductor under fretting condition.
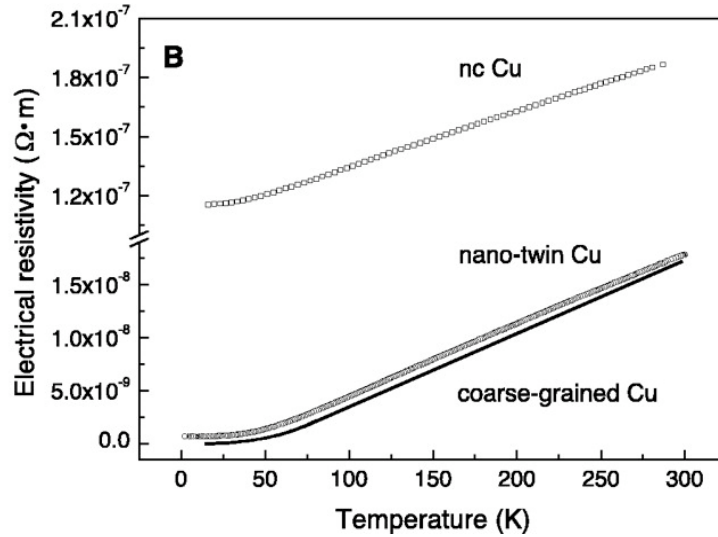
Figure 1.12 Temperature dependence of electrical resistivity for as-deposited nano-twined Cu, nanocrystalline and the coarse grained Cu in a temperature range from 2 to 296K [6].

1.6 Computer simulations on nanocrystalline Cu

After a series of experimental tests, nano-twinned Cu appears to have the best combination of mechanical properties and electrical conductivity. However, due to the limitation of experiment, the mechanical behavior of twin boundary at nanoscale is still not well understood. Instead, in this study, computer Molecular Dynamics simulation technique is used to look at the behavior of nano-twinning boundaries in terms of their mechanical properties. Computer modeling is more effective and easier to control

computational experiment's conditions. Simulation models can be constructed with different configurations to study effects of individual factors on the performance of a system. Computer simulation is particularly effective in studying systems at nanoscale. Atomistic simulation has been well demonstrated to be a useful tool to investigate material structures and corresponding mechanical properties at the nanoscale[10-13].

Attempts have been made to computationally investigate twinning at nanoscale. Wolf et al [24] studied deformation-induced twinning in nano Al; Cao et al[39-41] investigated tensile properties of nano wires containing twin boundaries, see Figure 1.13. Different densities of twin boundaries were added in nano wire Cu. The result of yielding stress demonstrated that adding twin boundary would increase materials strength. However, a nano wire contains a remarkable area of free surface. During simulation, dislocations are initiated from free surface and pile up at twin boundary. The stress concentrated at free surface area makes a large contribution to the resulting strength property. However, it is still hard to tell the mechanical behavior of a single twin boundary.
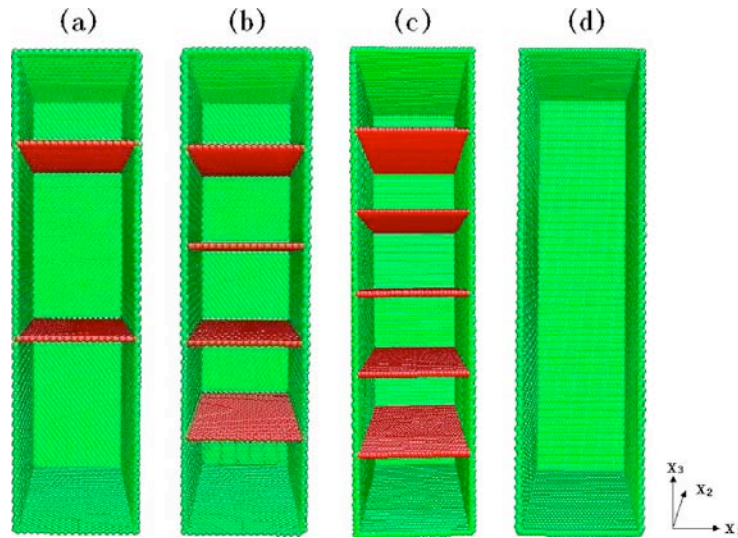
Figure 1.13 Configuration of (a) nanowire with two twin boundaries (b) nanowire with four twins (c) nanowire with five twins and (d) twin-free nanowire. Perfect FCC atoms and the front surface are not shown[40].

Li et al[42] discussed effects of twinning size on nano copper under shear strains. However, it is not well understood what would happen when the crystal size is extremely small, e.g., in the range where the inverse Hall-Petch relationship occurs in nanocrystalline structures, which is an issue still under debate. Nevertheless, efforts have been made to clarify relevant issues. Douglas et al [43] studied the tensile properties of grain boundary (tilted boundary, which is formed at the junction of differently oriented neighboring grains) in copper. Tschopp et al [44] looked at the nucleation of dislocations at different tilted grain boundaries. Shabib and Miller [45] investigated twin boundaries in large scaled nanocrystalline grains and associated toughness. Cao and Wei [41] studied the uniaxial tensile behavior of polycrystalline Cu.

Regardless of these efforts, for polycrystalline Cu, due to its large scale and different grain situations, it is difficult to study the effect of interior nano twinning on the mechanical behavior in detail.

1.7 Summary

Nano-twinned Cu is a good candidate for electrical contacts due to its high strength and low electrical resistivity. Although relevant experiments have been performed on nano-twinned samples, understanding the performance of nano-twinned Cu is difficult due to the limitation of existing experimental techniques. Computer simulation can be conducted under controllable computational experimental conditions, and is effective in investigating twin boundary mechanisms at nanoscale.

In this thesis study, nano-twinned Cu is studied through the molecular dynamics simulation with focus on the mechanical behavior. Single crystal and nanocrystalline Cu models are also studied for comparison purpose. Responses of the systems to one-directional and two-directional sliding processes are also investigated. The objectives of this thesis study are

1) to investigate the response of twin boundaries to stress at the nanoscale and the effect of interior nanotwinning on the mechanical behavior.

2) to look at responses of nano-twinned and nano-grained systems to external stress in the critical size range when inverse Hall-Petch

relation may occur.

3) to investigate the dislocation accumulation in nano-twinned system, in comparison with single crystal and nanocrystalline systems.

4) to study possible Bauschinger effect in two-directional sliding process.

Chapter 2 Simulation methodology

In the previous chapter, the advantage of employing molecular dynamics simulation for studying twin boundary mechanics properties is discussed. In this chapter, the details of simulation methods, algorithms for integrating Newton's equations, potential function, temperature and pressure control, energy minimization and order parameters will be provided and explained.

Molecular dynamics has a long history, dating from the statistical methods for studying large numbers of particles originated by Maxwell and Boltzmann[46]. Molecular dynamics simulation method was first introduced by Alder and Wainwright[47] in 1950's to study the dynamics of an assembly of hard spheres. This method could compute thermodynamic, structural and kinetic properties. The MD simulation method allows scientists study the motion of individual atoms, which is not possible in laboratory experiments. Soon it is widely used in the study of materials science.

MD simulation is more effective and easier to control computational experiment's conditions when material's size is down to nano scale, such as temperature and pressure. Details of temperature and pressure control will be introduced in the following chapter for a specific study. Although the MD simulation is powerful, limitations exist for computer simulation, i.e., limited system size. With the help of periodical boundary condition, the simulated system could be extended to "infinity". The time scale and the accuracy of the force fields limit MD simulation as well.

2.1 Newtonian mechanics

Molecular dynamics is a specialized computer simulation based on statistical mechanics. For a system of N molecules, the Hamiltonian H is a sum of kinetic and potential energy functions of a set of coordinates q and momenta p of each molecule i [48, 49]

$$H(p,q) = K(p) + V(q) \qquad \text{[2.1.1]}$$

For an N-atom interacting via a potential V, a classical equation of motion is given as follows

$$\frac{\partial}{\partial t}(\frac{\partial L}{\partial \dot{q}_k}) - \frac{\partial L}{\partial q_k} = 0 \qquad \text{[2.1.2]}$$

where the Lagrangian function is

$$L = K - V \qquad \text{[2.1.3]}$$

For a system of N atoms in Cartesian coordinates r_i,

$$m_i \ddot{r}_i - (-\nabla_{r_i} V) = 0 \qquad \text{[2.1.4]}$$

where m_i is the mass of the molecule i, which is assumed to be independent of position, velocity and time. r_i is a Cartesian coordinate and V represents inter-atomic potential. In the Newtonian interpretation of dynamics the translational motion of a spherical molecule i is caused by a force F_i. The motion and the applied force are explicitly related through Newton's second law:

$$F_i = m_i \ddot{r}_i \qquad \text{[2.1.5]}$$

$$F_i = -\nabla_{r_i} V \qquad\qquad [2.1.6]$$

The force on each atom is determined by interatomic potentials, with which acceleration of each atom could be calculated. Hence, integration of the equation of each atom yields the trajectory (positions, velocities and accelerations) of each atom as a function of time. Therefore, the initial position and velocity of individual atoms are the only data stored during MD simulation. From the equations, we could also tell that the interatomic potential V is a very important input for MD simulation. This will be discussed in section 2.3.

2.2 Algorithms for molecular dynamics

Regarding the Newton's equation of motion, how is the equation solved in practice? A standard method for ordinary differential equations is the finite difference approach. Given the molecular positions, velocities, and other dynamic information of an atom at time t, we attempt to obtain the positions, velocity etc. of the atom at time $t + \delta t$.

The Euler method, a first-order numerical procedure, is the most basic kind of numerical integration method, as shown below

$$r_i(t + \delta t) = r_i(t) + \dot{r}_i(t)\delta t \qquad\qquad [2.2.1]$$

and

$$v_i(t + \delta t) = \dot{r}_i(t) + \ddot{r}_i(t)\delta t \qquad\qquad [2.2.2]$$

Substituting Newton's law gives

$$v_i(t + \delta t) = v_i(t) + (-\frac{\partial V}{\partial r_i} \frac{\delta t}{m_i})$$ [2.2.3]

where r_i and v_i respectively represent position and velocity of atom i. t and δt are time and time interval. V is the employed force field and m_i is the mass of atom i. Thus the equations can be solved with given initial atoms positions, velocities and the inter-atomic potential. However, the first-order Euler method is not often used because it is less accurate than other higher-order algorithms.

One of the most commonly used integration algorithms is the Verlet algorithm[50]. The basic idea of such a algorithm is to write two third-order Taylor expansions for the particle position $r(t)$:

$$r(t + \delta t) = r(t) + v(t)\delta t + (1/2)\alpha(t)\delta t^2 + (1/6)b(t)\delta t^3 + O(\delta t^4)$$ [2.2.4]

and

$$r(t - \delta t) = r(t) - v(t)\delta t + (1/2)a(t)\delta t^2 - (1/6)b(t)\delta t^3 + O(\delta t^4)$$ [2.2.5]

where v, α, b, t are velocities, accelerations, the third derivatives of r with respect to t and time, respectively. O is the local error. Adding the two Eqn. [2.2.4] and [2.2.5] gives:

$$r(t + \delta t) = 2r(t) - r(t - \delta t) + a(t)\delta t^2 + O(\delta t^4)$$ [2.2.6]

Using Verlet algorithm, the local error in position of this algorithm is δt^4. However, in this algorithm, the velocities are not directly generated but obtained from positions.

$$v(t) = \frac{r(t + \delta t) - r(t - \delta t)}{2\delta t} + O(\delta t^2)$$ [2.2.7]

The accuracy of obtained velocity is only on the order of δt². To overcome this difficulty, Velocity-Verlet algorithm[50, 51], also called the leapfrog method, is developed, which has the form:

$$r(t + \delta t) = r(t) + v(t)\delta t + \frac{1}{2}a(t)\delta t^2 \qquad [2.2.8]$$

which includes two steps,

$$v(t + \frac{\delta t}{2}) = v(t) + \frac{1}{2}a(t)\delta t \qquad [2.2.9]$$

$$v(t + \delta t) = v(t + \frac{\delta t}{2}) + \frac{1}{2}a(t + \delta t)\delta t \qquad [2.2.10]$$

Compared to Verlet algorithm, Velocity Verlet algorithm has the same accuracy for predicting new atomic positions as Verlet algorithm does but has higher accuracy for velocity, up to δt^4.

The time step δt should be small enough to avoid discretization errors. In this study, the chosen time step is smaller than the fastest vibration frequency in the system, which refers to the vibration frequency of atoms, so that the motion of atoms, including thermally activated movements, can be captured. The typical order of the atomic vibrations frequencies is 10^{13} Hz. Thus, the time step used in this thesis is chosen to be $2*10^{-15}$ s.

2.3 Lennard-Jones potential and EAM potential

In section 2.1 we discussed the newton method. From Eqn. [2.1.4] and [2.1.5], one may see that, potential V is a very important input for simulation. Using different potentials influences the reliability of simulation results. Potentials frequently employed for simulation with respect to metals are pair

and many body potentials. The pair potential treats the overall energy of the system, as a sum of atomic pairwise interactions while many-body potential is the sum the energy contribution of three or more atoms.

Lennard-Jones 6-12 potential[52] is a classical pair potential shown as

$$V = 4\varepsilon((\frac{\sigma}{r})^{12} - (\frac{\sigma}{r})^6)$$
[2.3.1]

Lennard-Jones potential contains two terms, repulsion and attraction. Here, ε is the depth of the energy well and σ is the interparticle spacing when the pairwise potential equals zero. Lennard-Jones formula is convenient for simulation due to it simplicity, requiring less computer sources.

The many-body potential, as said above, is the sum of energy contribution of three or more atoms. Compared to pair potential, it involves more interactions other than the one between a pair of atoms. Therefore, many-body potential has a higher capability for describing atomic interactions while demanding more computing time. Embedded Atom Method potential[53] (EAM) is one of the important types of many body potentials. It is widely employed in simulations with metal materials since it introduces a local electron density term to the total potential energy. EAM potential is used in this thesis study.

EAM was firstly developed by Daw and Baskes[54] in 1984. EAM considers each atom in a solid as an impurity and all other atoms are viewed as the host in which the atom embedded. The energy of the impurity, the embedded energy, is a function of the background electron density. The energy of the host is a function of the impurity type and position. The total

potential energy is a sum of impurity and the host energy, expressed as:

$$E_{tot} = \sum_i F_i(\rho h, i) + \frac{1}{2}\sum_i \sum_{j \neq i} \phi_{ij}(R_{ij})$$
[2.3.2]

and

$$\rho h, i = \sum_{i \neq j} \rho_j^\alpha(R_{ij})$$
[2.3.3]

where $\rho h, i$ is the host electron density at atom i, $F_i(\rho h, i)$ is the embedded energy of atom i to electron density ρ. $\phi_{ij}(R_{ij})$ is pair-wise repulsion between atom i and j with a separation distance r_{ij}. For host electron density, $\rho_j^\alpha(R_{ij})$ is the contribution to electron density by atom j.

With the introduction of electron density, EAM potential has been proved to be an effective method to simulate metals. In this thesis, The atomic interactions are described using the Mishin[55] form of the EAM potential for copper. Compared to other EAM potentials, Mishin EAM potential is calibrated according to the *ab* initio values of stacking fault and twin formation energies. Thus more accurate simulation results could be obtained.

2.4 Temperature and pressure control

2.4.1 Temperature control

Classical MD simulation performs with microcanonical (NVE) ensemble, of which the number of atoms, volume of the system and total energy are conserved in simulation. In this thesis study, both tensile tests and sliding

tests are run at room temperature. During system initialization, the energy of the system is varied, while both volume and temperature are required to remain constant. Therefore, an adequate way is needed to control the system temperature.

Based on the classical NVE ensemble, the canonical ensemble (NVT) is the simplest extension. In this ensemble, the number of atoms, volume of the system and the temperature are fixed. The energy fluctuations are none-zero. The kinetic energy is related to temperature by the following equation,

$$\left\langle \sum_i \frac{1}{2} m v_i^2 \right\rangle = \frac{3}{2} N k_B T \qquad\qquad [2.4.1]$$

where m is the mass; v_i is the velocity; N is the number of atoms in system; k_B is the Boltzman constant and T represents the system temperature.

There are several methods to control system temperature for MD simulation. Nosé–Hoover thermostat is one of the classical types of such algorithms [56, 57]. The idea is to reduce the effect of the external system, acting as a heat reservoir. Energy exchange between the system and the reservoir is allowed, so that the reservoir can control the system's temperature. It introduces additional degrees of freedom to equation of motion, which allowed the equation of motion to be derived. The total energy of the simulation system plus the thermal reservoir is conserved.

In this thesis study, a rescaling velocity approach is employed, which controls the temperature by rescaling the atoms' velocity. At time step i, the instantaneous temperature is measured as T_i. A constant factor λ is used for

describe initial temperature T_0 and T_i, as shown

$$\lambda = \sqrt{\left(\frac{T_0}{T_i}\right)}$$
[2.4.2]

The variation of temperature ΔT can be presented as

$$\Delta T = \frac{1}{2}\sum_{i=1}2\frac{m_i(\lambda v_i)^2}{NK_B} - \frac{1}{2}\sum_{i=1}2\frac{m_i v_i^2}{NK_B}$$
[2.4.3]

m_i, v_i, are mass and velocity, N is number of atoms and K_B is Boltzman constant. With measured temperature and constant factor, velocities are rescaled to control the whole system remaining constant temperature.

2.4.2 Pressure control

In this thesis study, tensile test are performed under uniaxial loading. The sample's surfaces at tensile direction are controlled to fix at each tensile step, while the surfaces at the other two dimensions are controlled to be stress free. In MD simulation, the box size of test sample varied with time to sustain the stress free state, which means the pressure of the surfaces maintains zero. Therefore, the isothermal-isobaric constant (NPT) ensemble is chosen for the present study[58, 59]. To satisfy the constant pressure condition, a time-dependent metric tensor is introduced as an addition dynamical variable, which allow the volume and the shape of system to vary with time.

Suppose the simulation cell has N particles with an arbitrary shape described by three vectors *a, b* and *c. h* is the matrix formed by {*a,b,c*} and the

volume

$$\Omega = \|h\| = a \cdot (b \wedge c).$$ [2.4.4]

In order to describe the atoms positions of the simulation cell in the shape and size, besides the usual set of 3N dynamical variables, variability is augmented by the nine components of *h*. Thus the Hamiltonian is expressed as

$$H = \sum_i \frac{1}{2} m_i v_i^2 + \sum_i \sum_{j>i} \phi(r_{ij}) + \frac{1}{2} W Tr \dot{h}' \dot{h} + p\Omega$$ [2.4.5]

where the first two terms are kinetic and potential energy functions respectively, *W* is the mass with dimensions and *p* is the pressure. With Eqn. [2.4.5], the shape of simulation cell is allowed to vary and NPH ensemble is generated.

2.5 Simulation initialization and energy minimization

For constructing a simulation system, first the atoms are constructed with face-centered crystal structure in a Cartesian coordinate. After the configuration is input, each atom is randomly assigned velocity from a Maxwell distribution to obtain certain temperature, e.g., room temperature of 300K. Time step in MD simulation of this thesis was $2*10^{-15}$ second. Periodic boundary condition is employed in MD simulation of this thesis. In tensile test, the two edge planes normal to tensile direction are fixed boundary to control strain rate. In sliding test, the bottom boundary is fix while the top layer is set to be free surface. Details of boundary conditions will be

presented in latter chapters.

Energy minimization method[48] is used to bring a system from an unequilibrium to the local minimum energy state. The energy of system is minimized by iteratively adjusting atom coordinates. The total potential energy of the system could be express as a function of N atom coordinates:

$$E(r_1, r_2, ..., r_{N1}) = \sum_{i,j} E_{pair}(r_i r_j)$$ [2.5.1]

This function sums up all one-bonded pairwise interactions. The starting point for the energy minimization is the current configuration of the atoms. The minimization involves tool loops searching coordinates changing and evaluates force and energy. Conjugate gradient algorithm is used. Iterations are terminated when one of the stopping criteria is satisfied.

2.6 Order parameter

During the tensile and sliding processes, defects are generated. In order to analyze the deformation mechanism, a quantitative measure to distinguish the atoms that belong to grains, grain boundaries and other defects such as stacking faults and vacancies is required. The nature of the defects can be determined through the local arrangement of atoms. In this thesis, we use the bond-order parameter to identify the local structure around each atom. This bond-order parameter was first introduce by Steinhardt et al in 1984[60].

First, the neighbors of a molecule and bonds are defined. The bonds here

do not mean chemical bonds, but rather the unit vectors r_{ij} joining the center of mass of molecule i with the center of mass of neighbor molecules j within a given radius[60-62]. The orientation of the bond r_{ij} with respect to some reference coordinate system is specified by the spherical harmonics Y_{lm}, gives

$$Y_{lm}(r_{ij}) = Y_{lm}(\theta(r_{ij}), \phi(r_{ij})) \qquad [2.6.1]$$

where $\theta(r_{ij})$ and $\phi(r_{ij})$ are polar and azimuthal angles of vector r_{ij}. The global orientational order parameter $\bar{q}_{lm}$ of molecule i is defined by averaging over all bonds with its neighbors $N_{nb}(i)$,

$$\bar{q}_{lm}(i) = \frac{1}{N_{nb}(i)} \sum_{j=1}^{N_{nb}(i)} q_{lm}(i) \qquad [2.6.2]$$

The second-order invariants local order parameter $q_l(i)$ is expressed as

$$q_l(i) = \left[\frac{4\pi}{2l+1} \sum_{m=-l}^{l} |\bar{q}_{lm}(i)|^2 \right]^{1/2} \qquad [2.6.3]$$

the values of $q_4(i)$, $q_6(i)$ and $q_8(i)$ are listed in Table 2.1 for different local configurations.

Table 2.1 Values of $q_l(i)$ in different local configurations

Structure	Neighbor	$q_4(i)$	$q_6(i)$	$q_8(i)$
FCC	12	0.191	0.575	0.404
HCP	12	0.097	0.485	0.317
BCC	14	0.036	0.511	0.429

Based upon values of parameter $q_l(i)$ listed in table 2.1, different local

configurations (FCC, hexagonal close-packed 'HCP' and body-centered cubic 'BCC'), can be determined. For example, in FCC matrix, a partial dislocation along a [2] plane can be considered as a pair of HCP atomic layers (in red color), shown in Figure 2.1(a). This demonstrates an intrinsic stacking fault. Followed the same rules, see Figure 2.1(b) two single HCP layers are found in the FCC matrix. This means an extrinsic stacking fault, which is produced by interstitial agglomeration. Consequently, using this method we can distinguish atoms between the perfect crystal, grain boundaries, stacking faults, dislocations, and vacancies.

(a)

(b)
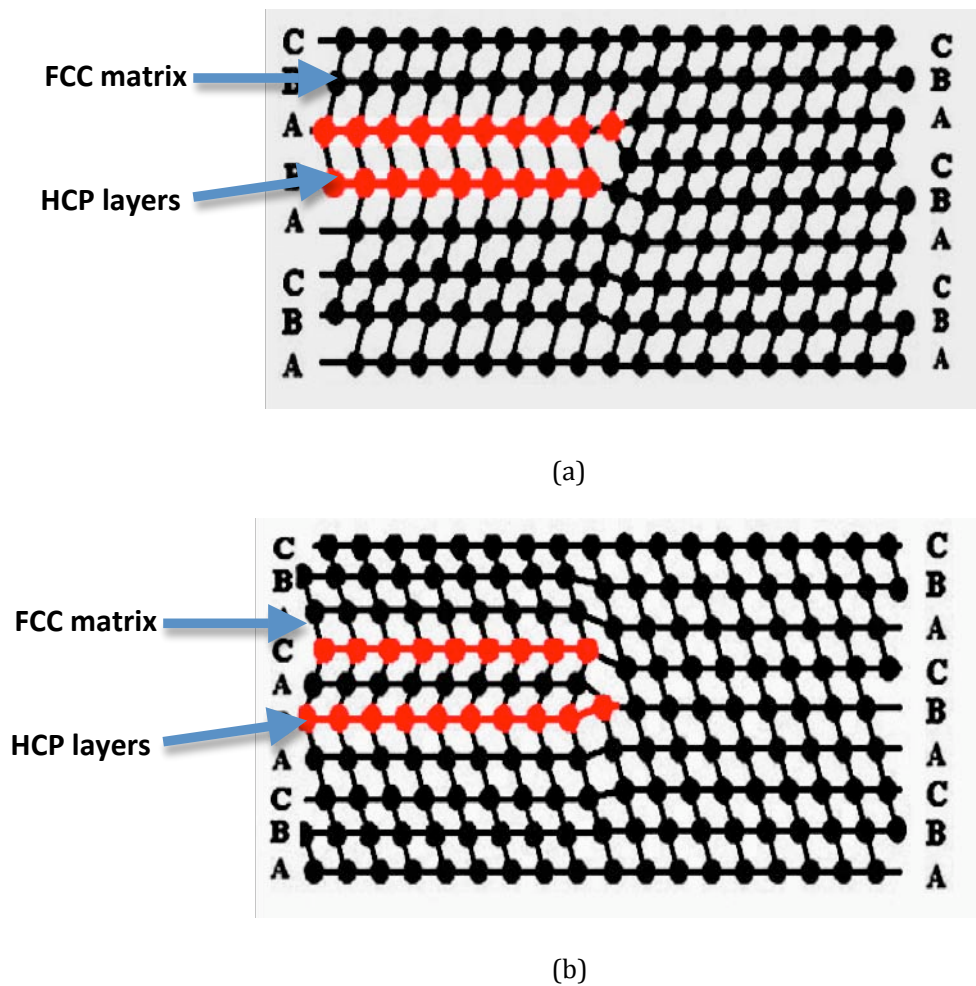
Figure 2.1 Stacking faults identified by order parameters. (a) An intrinsic

stacking fault. The HCP layers marked in red were detected in perfect FCC crystal. (b) An extrinsic stacking fault. Two HCP layers with a FCC layer in between.

2.7 Stress calculation

2.7.1 Stress tensor

During simulation, atomic stress is calculated to help understanding dislocation nucleation and mechanical response of material. The symmetric per-atom stress tensor has 6 components: xx, yy, zz, xy, xz, yz. EAM Potential introduced in section 2.3,expressed by Eqn. [2.3.2]. The force on atom *i* can be obtained from the total potential energy E_{tot} given in Eqn. [2.61]. X_i is the notation of atom *i*.

$$F_i = \frac{\partial E_{tot}}{\partial X_i} \tag{2.7.1}$$

combined with Eqn. [2.3.2]which yields

$$F_i = -\sum_{\substack{i=1 \\ i \neq j}} \left[\frac{\partial F_i}{\partial Ph,i} \frac{\partial Ph,i}{\partial R_{ij}} + \frac{\partial F_j}{\partial Ph,j} \frac{\partial Ph,i}{\partial R_{ij}} + \frac{\partial \phi_{ij}(R_{ij})}{\partial ij} \right] \hat{R}_{ij} \tag{2.7.2}$$

where $\hat{R}_{ij}$ denotes a unit vector along R_{ij}. The stress tensor can be obtained from the following form

$$P_{ab} = \frac{1}{V} \left[\sum_{i=1}^{N} \frac{P_{ia} P_{ib}}{m_i} - \sum_{\substack{i,j=1 \\ i<j}} (F'_i \rho h,j' + F'_j \rho h,i' + \phi'_{ij}) \frac{X_{ija} X_{ijb}}{R_{ij}} \right] \tag{2.7.3}$$

where V is the volume of the system, P_{ia} is the ath Cartesian component of the momentum of atom i. X_{ija} is the ath component relative position vector of atom i and j. Eqn. [2.7.3] sums up both the kinetic energy contribution for atom i and the pair-wise energy contribution.

2.7.2 Principle stress

As introduced above, during simulation, for each atom, 6 components of its stress xx, yy, zz, xy, xz, yz are calculated and stored in files, as shown in Figure 2.2. The material planes are perpendicular to the coordinate axes of a Cartesian coordinate system. With each plane, the stress tensor contains a normal component and two shear components. For example, the surface with normal vector in the direction of x-axis, the normal stress is denoted by σ_{xx}, and the two shear stresses are denoted as τ_{xy} and τ_{xz}. In this thesis, the mechanical response of nano copper under tension and sliding conditions is studied. Stress mapping is calculated for analyzing those mechanical behaviors, such as a tension stress concentration that could lead to a dislocation nucleation. Compared to the stress tensor introduced above, the principal stress has a simple form due to vanishing the shear stress component. Thus to have a better understanding of the model stress state, principal stress value is used to provide a clear view of stress state system.
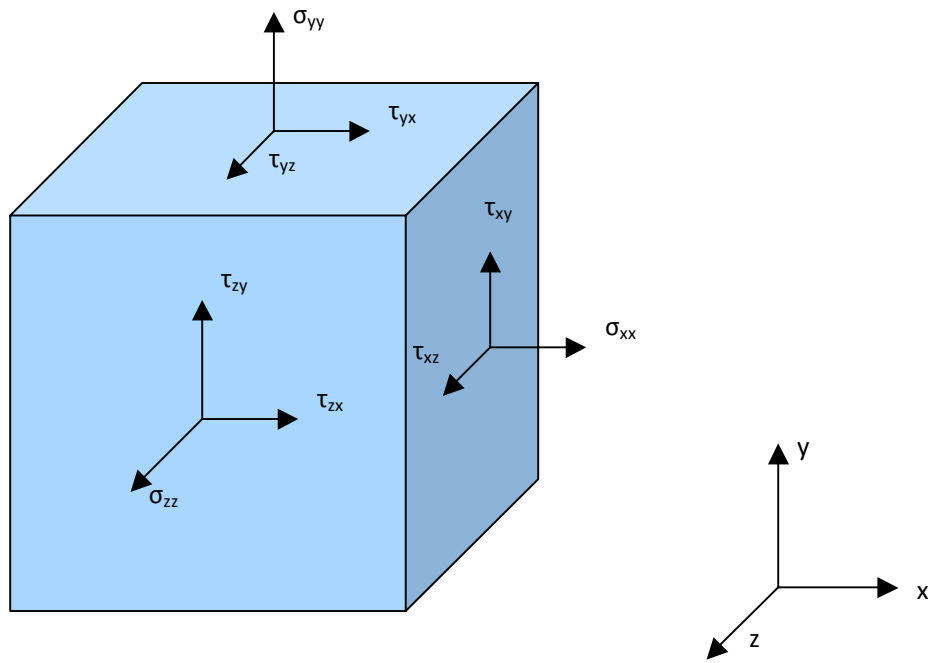
Figure 2.2 Components of stress in three dimensions.

In the tensor notation, the state of the stress, as shown in Fig 2.2, could be expressed as a three-by-three symmetric matrix.

$$T = \begin{bmatrix} \sigma_{xx} & \tau_{yx} & \tau_{zx} \\ \tau_{xy} & \sigma_{yy} & \tau_{zy} \\ \tau_{xz} & \tau_{yz} & \sigma_{zz} \end{bmatrix}$$
[2.7.4]

σ_{xx}, σ_{yy} and σ_{zz} are normal stress, and the rest are shear stress. To calculate the principal stress is to vanishing the shear stress. Thus the problem of finding the principal stresses turned out to that for finding eigenvalues. σ_1, σ_2, σ_3 are used to present principal stresses, $\sigma_1 > \sigma_2 > \sigma_3$.

$$A = \sigma_{xx} + \sigma_{yy} + \sigma_{zz}$$

$$B = \sigma_{xx}\sigma_{yy} + \sigma_{yy}\sigma_{zz} + \sigma_{zz}\sigma_{xx} - \tau^2_{xy} - \tau^2_{yz} - \tau^2_{xz} \qquad \text{[2.7.5]}$$

$$C = \sigma_{xx}\sigma_{yy}\sigma_{zz} + 2\tau_{xy}\tau_{yz}\tau_{xz} - \sigma_{xx}\tau^2_{yz} - \sigma_{yy}\tau^2_{xz} - \sigma_{zz}\tau^2_{xy}$$

where A, B and C are coefficients. Therefore the three roots of Equation are
σ'_1, σ'_2 and σ'_3, one has the following equations:

$$\sigma'_1 + \sigma'_2 + \sigma'_3 = A$$

$$\sigma'_1\sigma'_2 + \sigma'_2\sigma'_3 + \sigma'_1\sigma'_3 = B \qquad \text{[2.7.6]}$$

$$\sigma'_1\sigma'_2\sigma'_3 = C$$

Numerically, the three roots of Equation [2.7.4] can be found. In this thesis
study, matlab is used to solve such eigenvalue equations. After obtaining the
values, one may re-order the three roots and obtain the principal stresses.

$$\sigma_1 = \max(\sigma'_1 \sigma'_2 \sigma'_3)$$

$$\sigma_3 = \min(\sigma'_1 \sigma'_2 \sigma'_3) \qquad \text{[2.7.7]}$$

$$\sigma_2 = A - \sigma'_1 - \sigma'_3$$

Chapter 3 Responses of twin boundaries to tensile stress

In the previous chapter, details of algorithms for integrating Newton's equations, potential function, temperature and pressure control, energy minimization and order parameter are presented. With the help of computer and these algorithms, simulation can be conducted.

In this chapter, computational results of tensile responses of twin boundaries in comparison with single crystal and grain boundaries in Cu are presented. The atomic interactions were described using the Mishin form of the Embedded Atom Method [53] (EAM) potential for Cu. The simulations were performed within a NPT ensemble (fixed numbers of atoms, pressure and temperature). Whole tensile process was run under room temperature controlled by rescaling velocity scheme. Three different types of models were selected, nano-twined, single crystal and nano-grained model systems. The grain size is range from 5 to 20 nm where the inverse Hall-Petch relation (H-P) may occur in nanocrystalline copper. The total number of atoms is varied from 44663 to 101135. MD Simulations were performed using large-scale atomic/molecular massively parallel simulator (LAMMPS)[63], developed by Sandia National Laboratory. The purpose of simulation is to get a better understanding of the general mechanical behavior when nano-twin boundary under tensile stress.

In the following sessions, the simulation geometry, system initialization and tension process are described. Obtained results suggest that the twin boundary blocks dislocation movement more effectively and the degree of emitting dislocations under stress is considerably lower than that of grain boundary, leading to superior mechanical behavior. The inverse H-P relation is not applicable to the nano-twinned system. Besides, it is also demonstrated that the inverse H-P relation occurring in nano-grained materials does not necessarily result from grain boundary sliding.

3.1 Simulation geometry

In tensile simulation, we looked at three model systems in total, including single crystal, one crystal with two twin boundaries (nano-twinned), and one with two grain boundaries (nano-grained) as illustrated in Figure 3.1 (a) (b) and (c). All these models are constructed with the same orientation along the tensile direction. For the system with twin boundaries, the initial configuration is constructed by repeating $\Sigma 3$ coherent twin boundaries with their normal parallel to the <111> axis (in the direction along which the external force is applied). To construct the grain boundary, we twisted a $\Sigma 7$ boundary and then added 1% vacancies i.e. took off 1% atoms randomly from the boundary area. The crystals at two sides of the boundary had their <112> and <110> parallel to the Y and the Z coordinate directions, respectively.

In order to study the size effect on the response of the systems to stress applied, six different system sizes are used, varied from 5nm to 25nm for the spacing between two adjacent boundaries. For single crystal, because it does not contain any boundaries, it was constructed with the same system size as nano-twinned and nano-grained models. Therefore, a 5nm single crystal model means the same system size as 5nm nano-twinned model system. The system size with a grain of 5nm in the middle is 15.9nmx9.35nmx3.5 nm, which has about 45000 atoms. Details of size information are listed in Table 3.1.
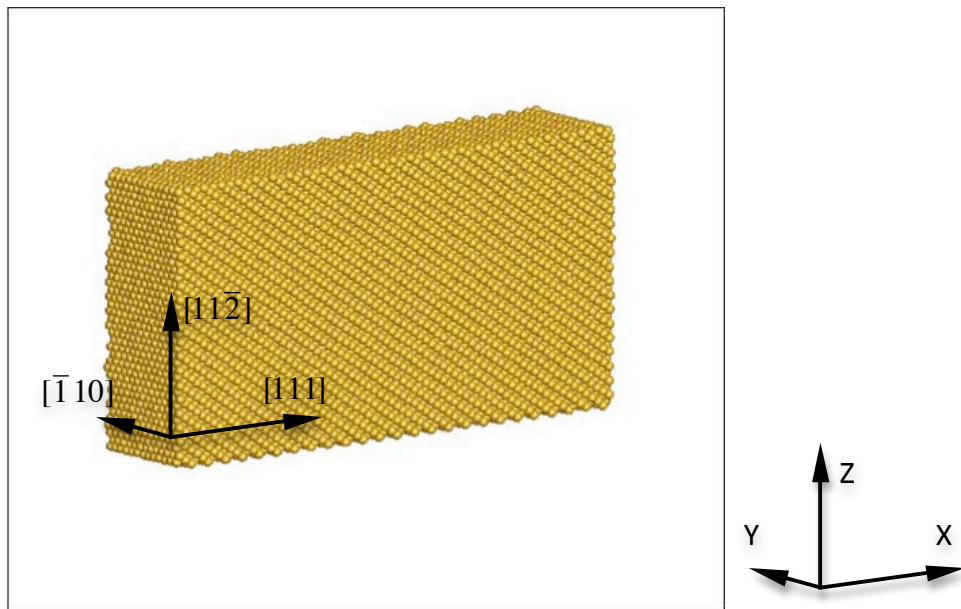
(a)
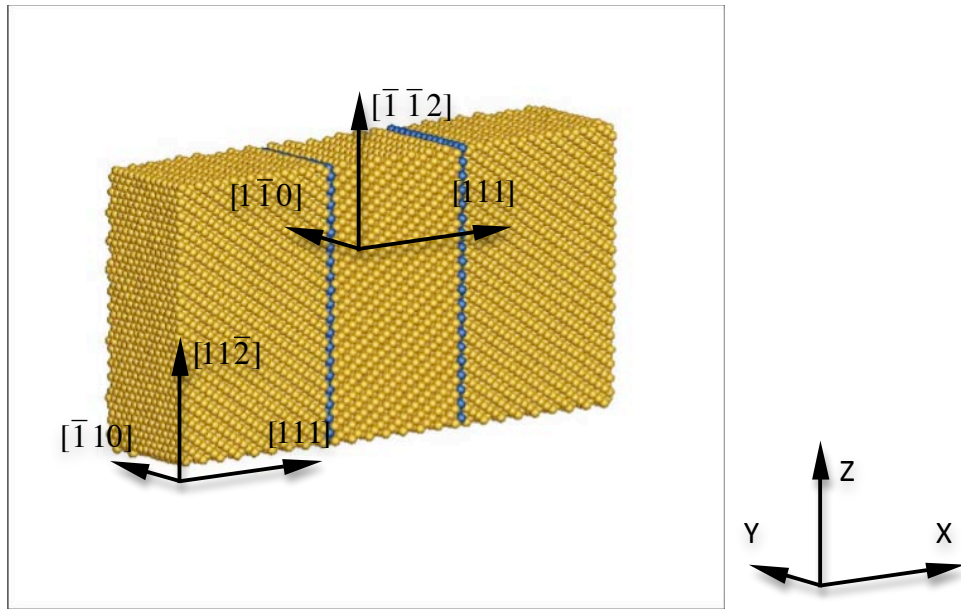
(b)
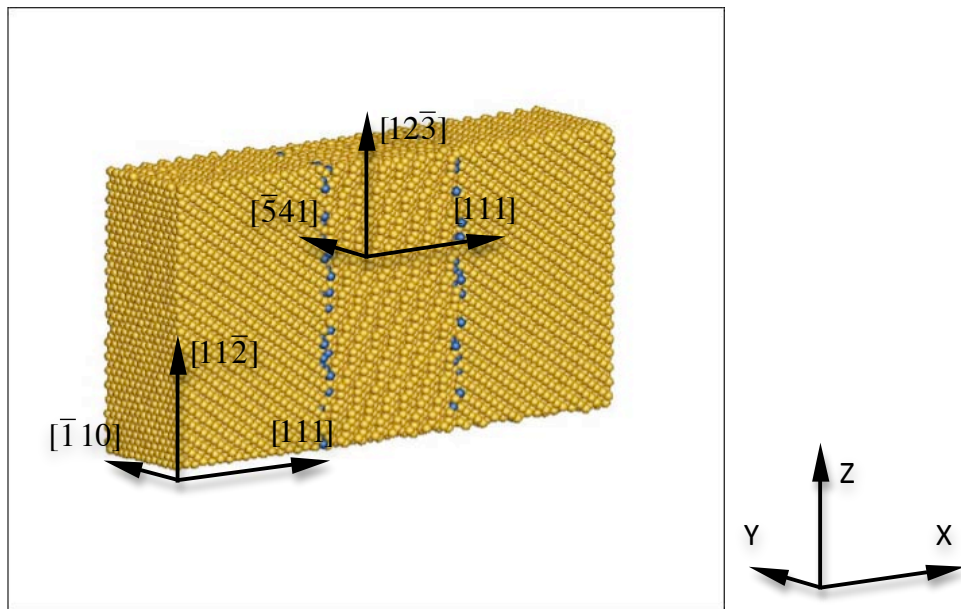
(c)

Figure 3.1 Three model systems: (a) one single crystal, (b) one crystal with two twin boundaries (nano-twinned), and (c) one crystal with two grain boundaries (nano-grained).

Table 3.1 Number of atoms and system sizes

Spacing between boundaries		5nm	7.5nm	10 nm	15 nm	20 nm	25 nm
Number of atoms in system	Nano-twinned/ Single crystal	44687	51743	58799	72911	87024	101135
	Nano-grained	44663	51719	58775	72887	87000	101111
System geometry (nm*nm*nm)		15.9*9.35*3.5	18.4*9.35*3.5	20.9*9.35*3.5	25.9*9.35*3.5	30.9*9.35*3.5	35.9*9.35*3.5

3.2 System relaxation

After the initial construction, all systems need to be relaxed before performing tensile simulation process. The single crystal and twin boundary model systems are thermally equilibrated to 300K for 500ps, shown in Figure 3.2 (a)(b). Relaxation is run within a NVT ensemble. Temperature is controlled using velocity-rescaling method. For grain boundary model system, when constructing the initial structure, vacancies have been taken from boundary area. In order to have the GB model system closer to the reality, the initially constructed system is first heated up to 900K for 100ps, and then gradually cooled down to the room temperature (300K), see Figure 3.2(c). The system reaches local minimum energy state using energy

minimization method, which has been introduced in chapter 2. The potential

energy curve shows fluctuation become smaller, and the value become stable

during relaxing period. Periodical boundary condition is utilized in the Y-, Z-

directions and free surface in X- direction.
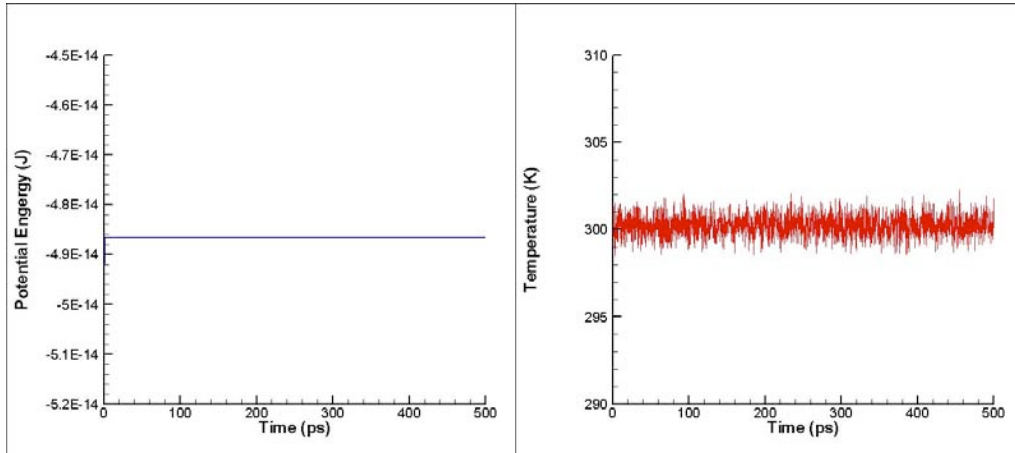
(a)
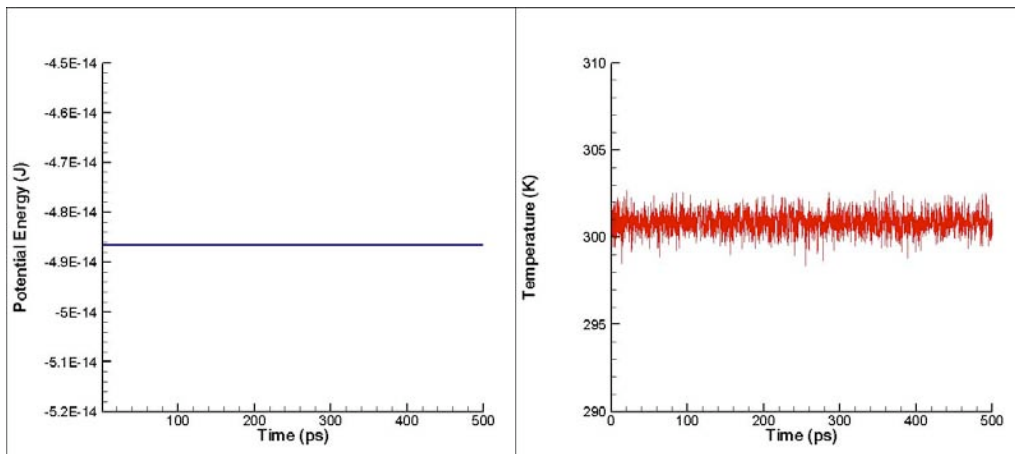
(b)
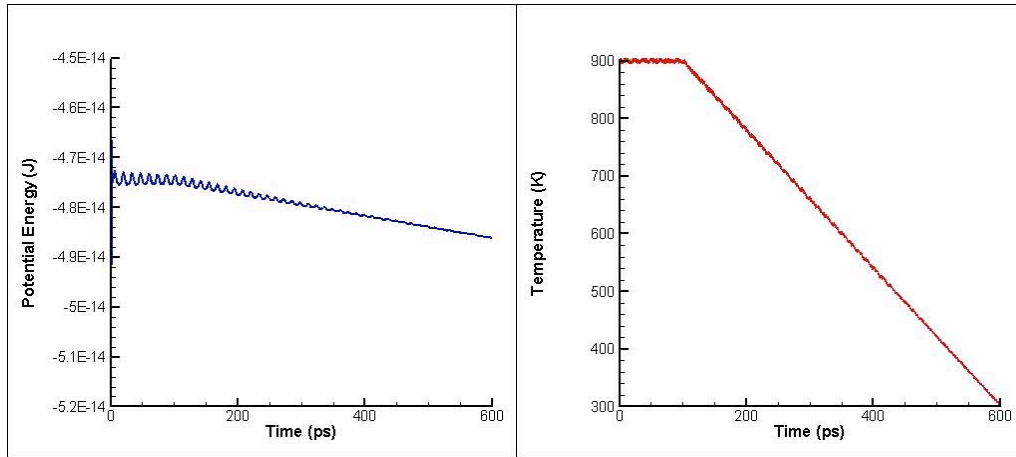
(c)

Figure 3.2 Relaxing energy and temperature of (a) single crystal model system (b) twin boundary model system (c) grain boundary model system (the spacing between two ends of the system is 20 nm)

3.3 Apply tensile loading

The relaxed models then perform tensile simulations. Uniaxial tensile loading is applied to each system along the X direction (parallel to <111> crystallographic direction) until the model system gets failed. During the tensile test, three atomic layers at one end of a simulated system are fixed throughout the entire tensile process, while three atomic layers at the other end are pulled at a constant tensile speed. Periodical boundary condition is utilized in the Y-, Z- directions. The loading rate is about 10^7 s^{-1}, which is rather slow for MD simulation. The entire tensile process proceeds at a constant temperature of 300K using velocity rescaling thermostat. The atomic interactions are described using the Mishin[55] form of the Embedded Atom Method [53] (EAM) potential for Cu.

3.4 Results and discussion

Using the above-described systems and loading procedure, computational tensile tests for the three different model systems are performed; corresponding stress-strain (σ-ε) curves are obtained. As an example, Figure 3.3 illustrates (σ-ε) curves of the three systems with the spacing of 10 nm between two adjacent boundaries. The following phenomena are observed and related mechanical behavior was investigated.

3.4.1 Elastic behavior and yielding

As shown in Figure 3.3, all three tensile curves have the same slope in the elastic deformation region, indicating that they have the same elastic modulus or Young's modulus, which is about 163 GPa along the <111> crystallographic direction. It is known that the elastic modulus is an intrinsic property of a solid, which is determined by its atomic bond strength and crystal structure. The elastic modulus should be affected by interfaces such as grain boundaries. However, since the volume of grain boundaries in a polycrystalline solid is very small, the interfacial influence on the elastic modulus is thus negligible. Even in nanocrystalline solids, the volume fraction of grain boundaries is still small unless the grain boundaries are diffuse or thick such as those observed in metals or alloys experienced severe plastic deformation without recovery treatment. As shown in the present

simulated nano-systems (see Figure 3.1), the twin and grain boundaries only take very small volumes of the systems. Thus, influences of the boundaries on the elastic modulus are not expected to have significant influence on the elastic modulus.

However, the influence of the boundaries on the yield stress or strength is pronounced, since they affect the generation of dislocations. As shown in Figure 3.3, after elastic deformation, the curves show precipitous drops corresponding to the occurrence of yielding or plastic deformation. Yielding stresses of the single crystal and one with two twin boundaries are 12.2 and 12.4GPa, respectively; while the one with GBs showed a lower yielding stress of 11.6GPa. It should be indicated that in realistic situation, materials contain a very large number of grain boundaries or twin boundaries. Thus the difference in the yielding stress between materials containing twin boundaries and those containing grain boundaries would be significantly amplified, especially for nanocrystalline and nano-twinned materials as evidenced by experimental observations[6].
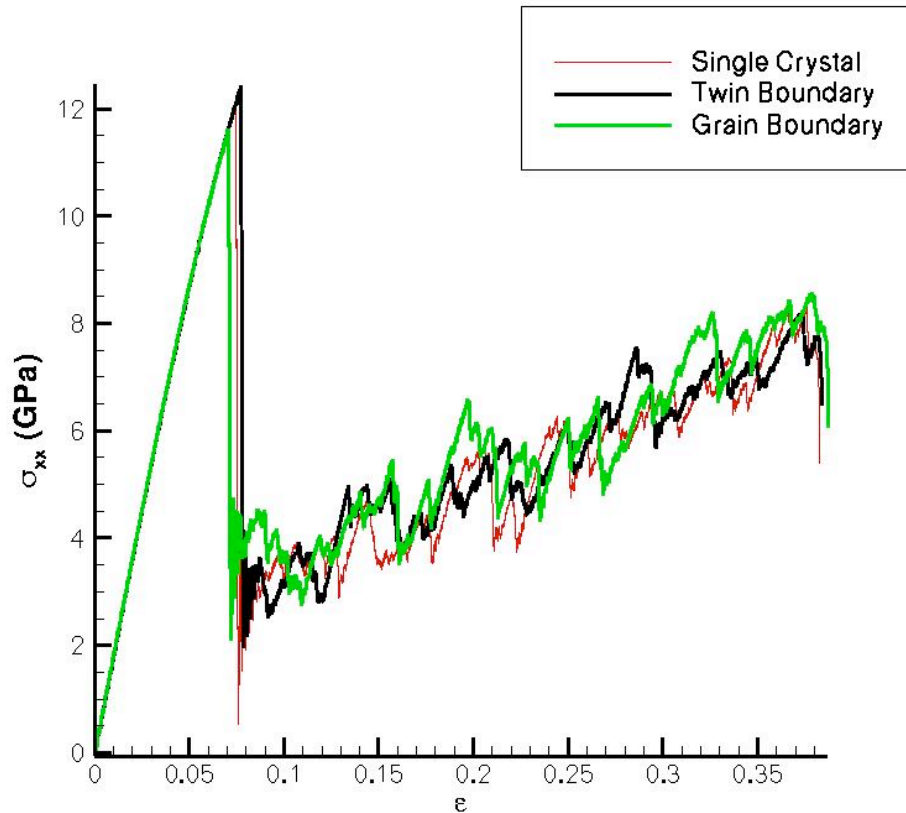
Figure 3.3 (σ-ε) curves of the three systems with the spacing of 10 nm between two adjacent boundaries (for the single crystal, the spacing between two ends of the system is 10 nm)

In order to obtain more detailed information for better understanding of the difference in the mechanical behavior among the systems under study, we look at distributions of stress or lattice distortion in the three systems prior to yielding. A few snapshots are taken just before yielding; the local stress distribution is illustrated in Figure 3.4, in which colored atoms are used to reflect the local stress magnitude. As the color bar shows, red color

stands for higher stress than the green. As illustrated, the single crystal and nano-twinned systems show spread stress distribution of relatively low magnitude with only one spot having higher stress concentration inside crystal, at which plastic deformation is initiated. While the system with grain boundaries shows many higher stress spots along the grain boundaries. This may also be seen in Figure 3.4 (d) (e) and (f), which illustrate the lattice distortion inside the single crystal and around boundaries with spots of high stress concentrations. The local atomic arrangement in the distorted regions reflects the generation and emission of partial dislocations, which are all formed on {111} plane, slipping along $<11\overline{2}>$ direction (identified through calculating the orientation of generated partial dislocations). In Figure 3.4 (d) and (e), the distorted regions are marked, in which dislocations are generated from inside crystal in the single crystal and nano-twinned systems; while in the system with grain boundaries dislocations are emitted from grain boundaries as Figure 3.4 (f) illustrates. It is known that the grain boundary has a disordered structure with some free space or vacancies, which render the grain boundary to have higher strain energy. Such an interfacial imperfection generates a preferential region of emitting dislocations when external stress is applied. Plastic deformation is easier to be initiated in a polycrystalline solid than in a perfect crystal of the same material, although the former is macroscopically harder due to the fact that grain boundaries block dislocation movement. It needs to be pointed out that the local initiation of plastic deformation may not reflect the macroscopic

yield strength. This happens because when yielding becomes macroscopically visible, the dislocation movement has been considerably active and thus the barriers such as grain boundaries to dislocation movement could become a dominant factor affecting the apparent yielding strength of a material. At the nano scale, the situation is somewhat different when the nucleation of dislocations plays an important role in local initiation of plastic deformation.
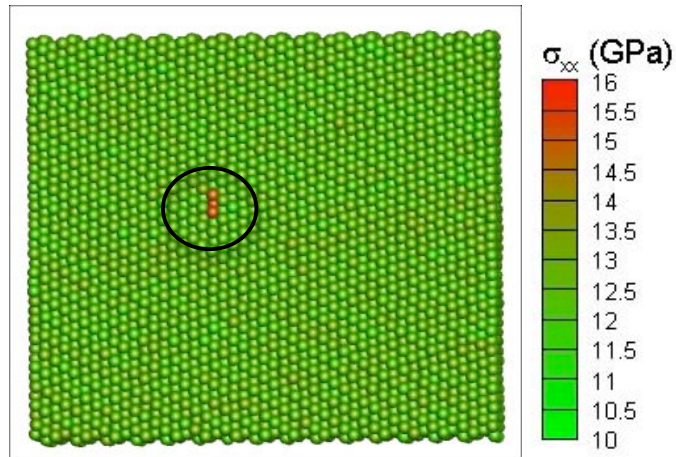
(a)
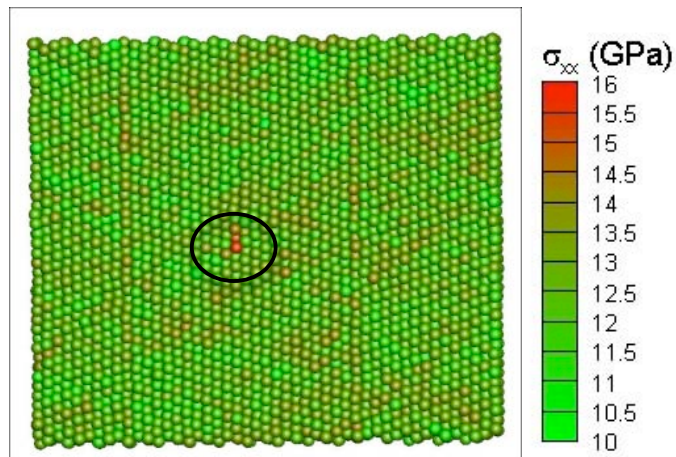
(b)
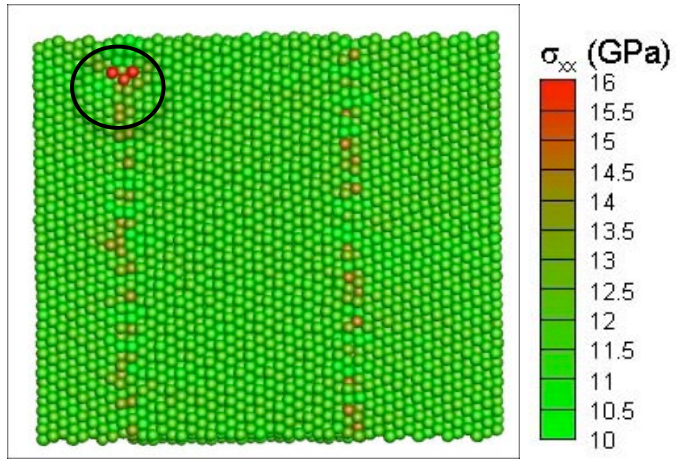
(c)
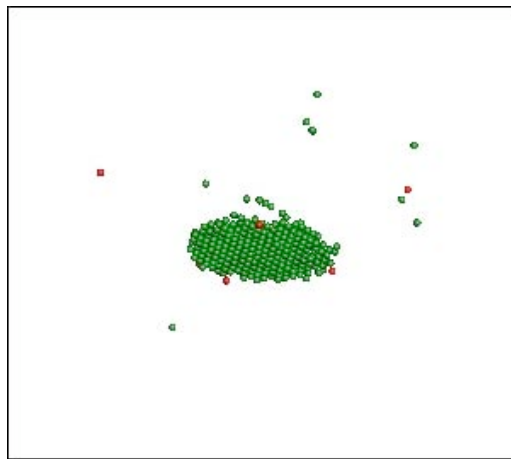
(d)
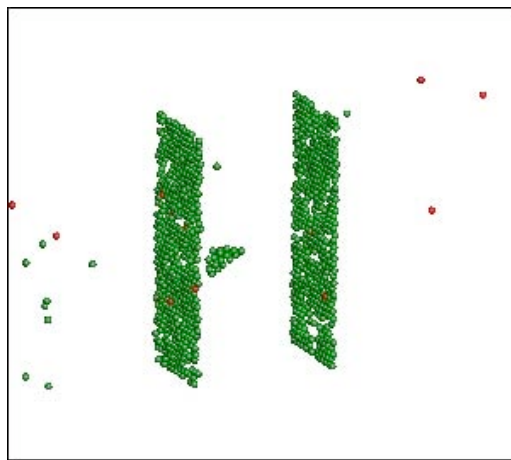
(e)
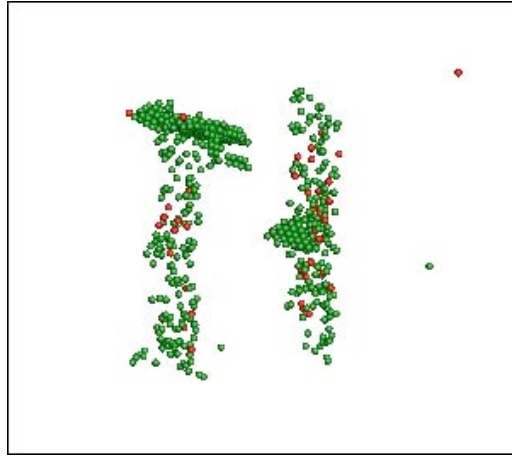
(f)

Figure 3.4 Stress distributions just before yielding: (a) single crystal, (b) a system with two twin boundaries, and (c) a system with two grain boundaries. Colored atoms are used to reflect the local stress magnitude. (d), (e) and (f) illustrate the lattice distortion and spots of high stress concentrations in the three systems, respectively, where plastic deformation is likely initiated.

With regard to the twin boundary, although it also generates mismatch strain with a certain interfacial energy, its ordered structure has lower interfacial energy compared to that of the grain boundary, which makes dislocations difficult to be generated or emitted from the twin boundary under external stress. Therefore, the twinned system may behave in a manner similar to that of the single crystal system. The simulation demonstrates that the grain boundary structure is weaker than the twin

boundary and perfect single crystal, corresponding to a lower yield stress at which dislocations are emitted. Or in other words, the dislocation emission is easier at grain boundaries than at the twin boundary or inside a single crystal.

Compared to the single crystal system, the nano-twinned system has slightly higher stress magnitude though the stress is well spread. This makes the former to have slightly higher yield stress.

3.4.2 Effect of the crystal size on the yield strength

The yield strength is directly related to the dislocation nucleation and the barrier to its movement as well. When the free path for dislocations to move is small, the yield strength is influenced. In this simulation study, we investigate the effect of grain size on the yield strength by determining the yield strength as a function of the spacing between two boundaries that was decreased from 25 nm to 5 nm. For the single crystal system, since there is no boundary inside, the size of the entire system was kept to be the same as those of other systems containing boundaries. As illustrated in Figure 3.5, with a decrease in the grain size, the single and twin boundary systems show slightly increase in the yield strength. However, the system with grain boundaries initially increased to larger degree but started to decrease as the spacing was reduced to about 10 nm, consistent with studies reported in literature[64].
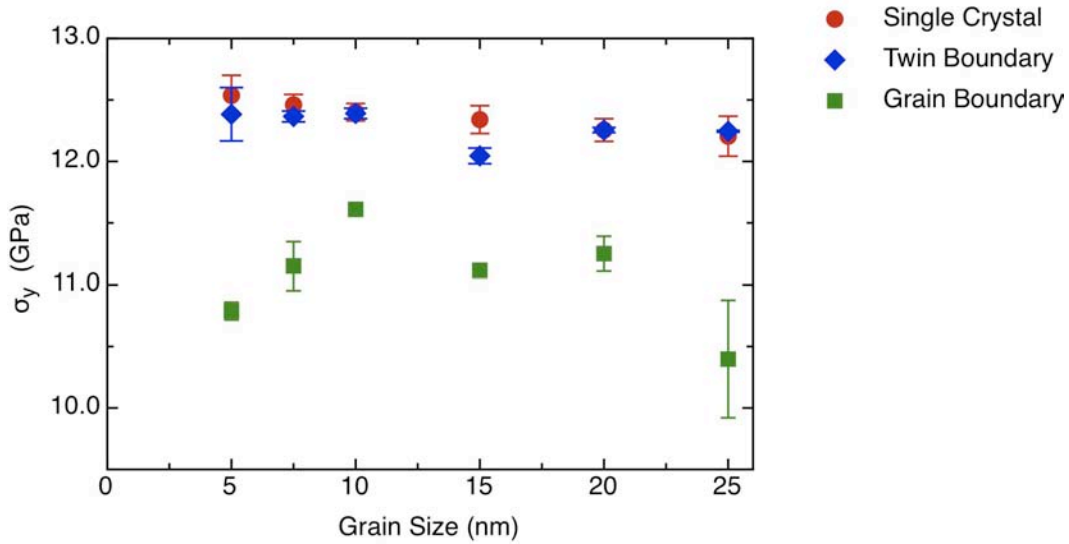
Figure 3.5 Variations in the yield strength with respect to the grain size of the three model systems.

It is known that as the grain size decreases, the yield strength increases as the Hall-Petch equation, $\sigma_y = \sigma_\circ + kd^{-1/2}$, describes. However, when the grain size is sufficiently small, usually below 8 ~ 10 nm, the influence of the grain size on σ_y is reversed, following the so-called inverse Hall-Petch relationship[65]. Such softening is ascribed as grain boundary sliding[31-35]; but there is no direct experimental confirmation. In the present study, the applied stress is uniaxial and vertical to the grain boundaries while the surface layers of two ends of the systems are set to be rigid during the tensile process, thus we assume there is no grain boundary sliding.

In order to figure out whether the reverse Hall-Petch relationship is caused by grain boundary sliding, we perform a simulation tracking the mass

center of each grain, see Figure 3.6.
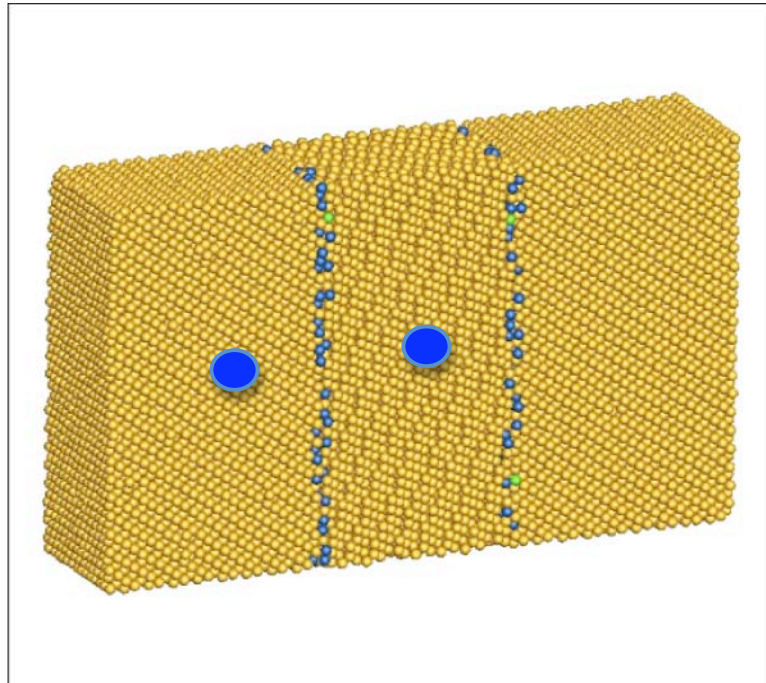
Figure 3.6 Mass centers in each grain of grain boundary model system

A certain amount of atoms that are far away from boundaries and edge areas are selected to calculate the grain mass, presented by blue spot in Figure 3.6. Tracking the mass center trajectory we get the relative displacement between two mass centers shown in Figure 3.7.
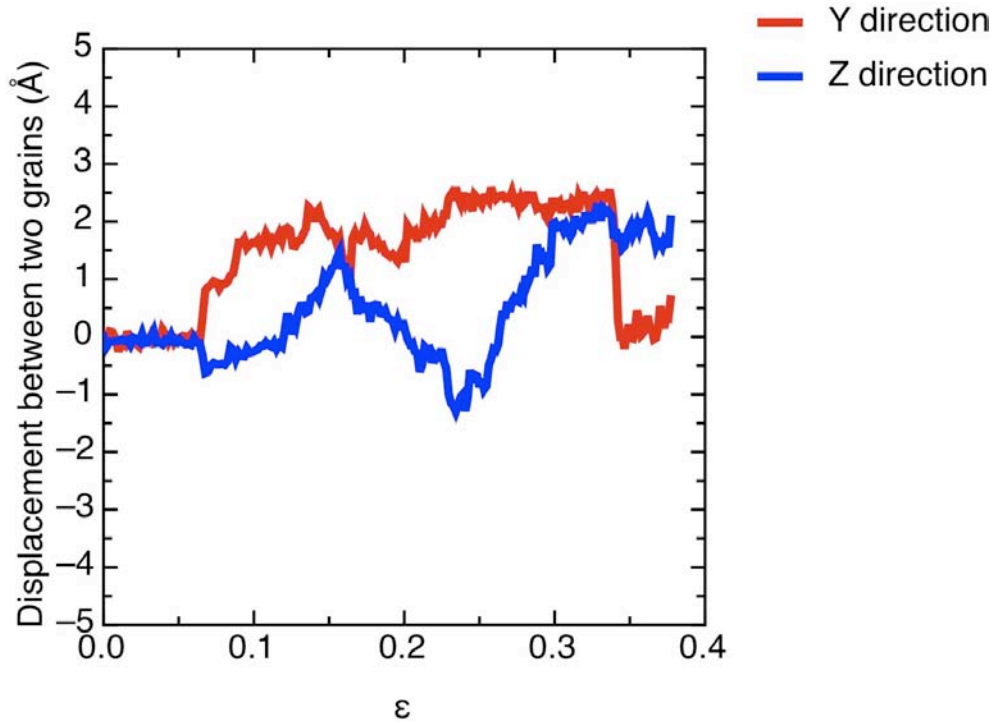
Figure 3.7 Displacement between two mass centers in grain boundary system.

As shown, no obvious movement is observed. The fluctuations reflect the dislocation nucleation and movement inside the grain, but not from the grain boundary sliding. Thus, the obtained results from the simulation suggest that the inverse Hall-Petch relationship does not necessarily result from grain boundary sliding.

The disordered grain boundary plays a dual role, acting as both a sink and a source of dislocations. Although a GB blocks the movement of dislocations, it emits or releases dislocations under stress with a relatively lower energy barrier, compared to that for generating dislocations inside a perfect crystal. There is competition between these two opposite functions

during yielding. When the grain size is very small, the emission of dislocations could become predominant as the distorted zones in the vicinity of grain boundaries with interfacial stress overlap or are close enough so that the dislocation emission and migration could be facilitated, leading to a decrease in σ_y, corresponding to the occurrence of the inverse H-P relation.

It is debated that when the grains are extremely small, e.g., < 10 nm, dislocations may not operate within grains or crystals. However, the present study demonstrates the existence of dislocation emission and spreading in the crystal under applied tensile force for all crystal sizes under study (see Figure 3.8). As shown, in the nano-grained system, dislocations are generated at grain boundaries and then spread over the system; in the single crystal and the twinned system, dislocations are initially generated inside crystal and then spread over the entire space.

The inverse Hall-Petch relationship was not observed during simulated tensile tests for systems with twin boundaries, as shown in Figure 3.5. Based on the above argument, the inverse Hall-Petch relationship may not be applicable to the nano-twinned systems, since the twin boundary is ordered, which should have a considerably larger energy barrier to dislocation emission, compared to the GB (see Figure 3.8, in the nano-twinned system, dislocations are generated inside the crystal rather than at twin boundaries). Thus, acting as an obstacle to dislocations more than a source for dislocation emission, the twin boundary will be more effective to stop the dislocation movement as its density increases, leading to

an increase in σ_y as shown in Figure 3.5.

As for the simulated single crystal systems, when the spacing between two rigid ends of a single system varies by changing the number of fixed atomic layers at the ends, the situation is similar to that of the twin boundary system, since the fixed atomic layers do not emit dislocation but stop dislocation movement. Thus, the single crystal systems with different crystal sizes behave in a manner that is similar to the nano-twinned system.

(a)

(b)

(c)
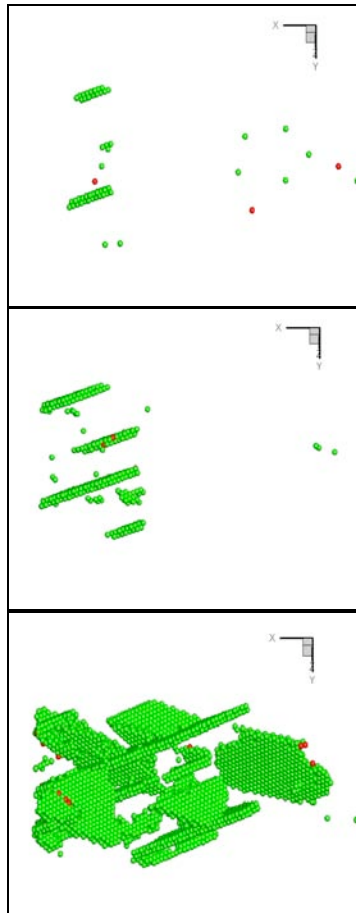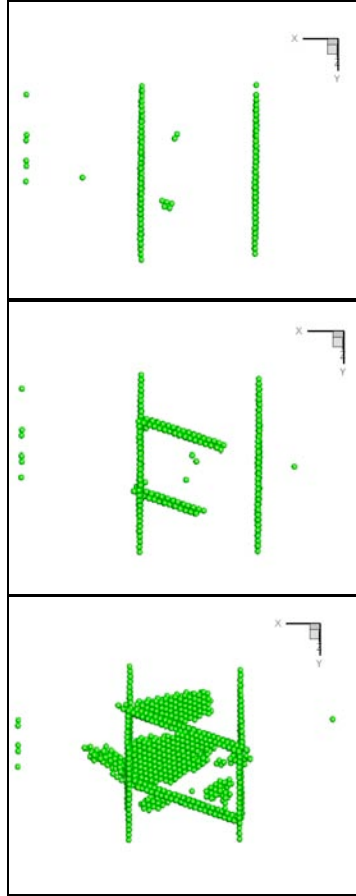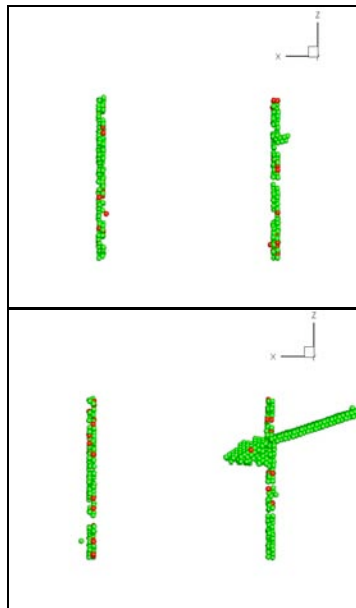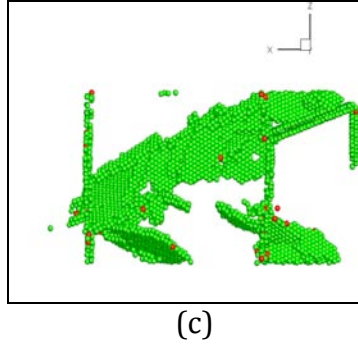
Figure 3.8 Processes (from top to bottom) of dislocation emission and spreading in crystal under stress for the three systems: (a) single crystal, (b) nano-twinned, and (c) nano-grained model systems. As shown, in the nano-grained system, dislocations are generated at grain boundaries; while in the single crystal and TB system, dislocations are initially generated inside crystal and then spread.

3.4.3 Energy absorption and failure

The strain energy absorbed by a solid before failure is a measure of its toughness. At nanoscale, it may be more appropriate to describe toughness directly as the energy absorption capability i.e. [✗] , which is determined by both the strength and ductility. U values of the three different systems are calculated. Figure 3.9 shows locations of fracture in the three systems. As shown, in both systems with twin and grain boundaries, fracture occurs at the boundaries, which block dislocation movement and generate high stress concentrations that contribute to the failure. As for the single

66

crystal system, fracture occurs near the fixed end of the system, where dislocations are also blocked. The energy absorption is calculated for the entire deformation process before fracture. In this case, the situation is more complicated, involving dislocation nucleation and propagation. U depends on both the stress and the ductility or the failure strain, ε_f, which is shown in Figure 3.10. As shown, the ductility is almost the same for all the three systems when the grain size is above 10 nm, below which the system with grain boundaries shows larger ε_f compared to the nano-twinned system but the single crystal has the largest ε_f, although the data scattering becomes larger. These could be explained. For the single crystal, there is no boundary inside the system to block dislocation movement, corresponding to higher ductility. Compared to the twin boundary, the grain boundary may emit dislocations more easily and block dislocations less effectively; these may render the GB-containing system is more flexible than the TW-containing system. Figure 3.11 presents variations in U for all the three systems with respect to the crystal size. As shown, with a decrease in the crystal size, U increases for all the three systems. During the loading process, after yielding the interaction among dislocations and that between the dislocations and interfaces are enhanced as the stress is continuously increased. All three systems show the strain-hardening effect (see Figure 3.3). As the crystal size decreases, the confinement of dislocations by the twin and grain boundaries is enhanced, resulting in an increase in U. The nano-twinned system shows

slightly higher U value, because prior to fracture the twin boundaries block dislocation movement more effectively with a lower degree of dislocation emission, compared to the system with grain boundaries. As for the single crystal system, the dislocations are constrained by the two rigid ends or rigid surface layers at the ends, on to which the external stress is applied, so that the confinement is also enhanced as the system size is reduced.

(a)   (b)

(c)
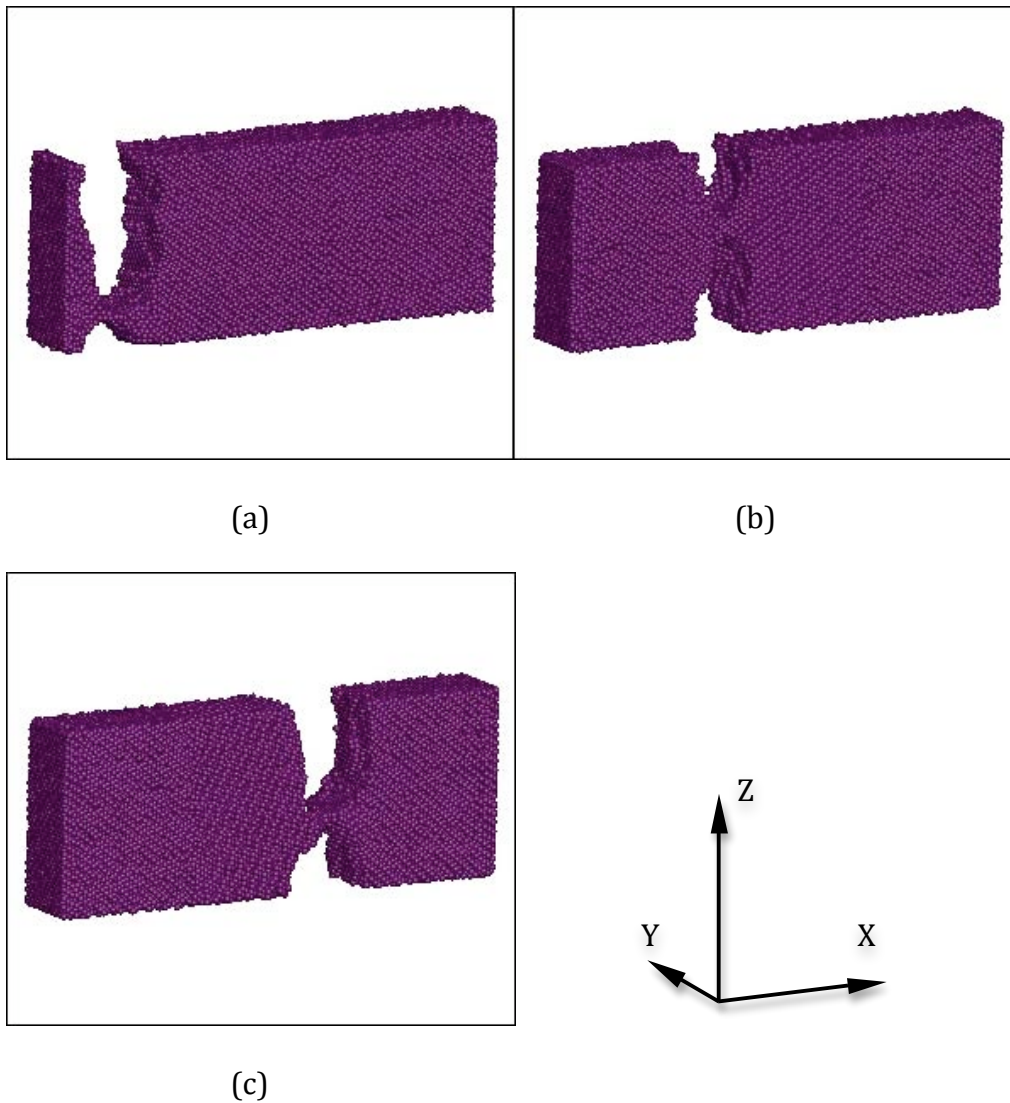
Figure 3.9 locations of fracture in the three systems: (a) single crystal model system (b) twin boundary model system (c) grain boundary model

system

As the crystal size is smaller than about 10 nm, the situation changes. U values of both systems with twin and grain boundaries decrease with decreasing the crystal size largely due to the decrease in ductility. The single crystal does not show such an obvious change.
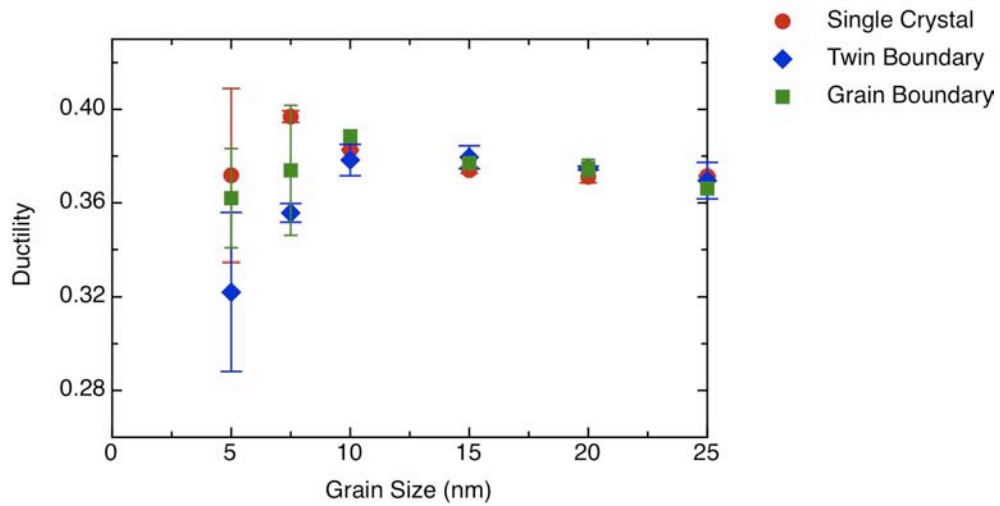
Figure 3.10 Ductility vs. the grain size for the three simulated systems
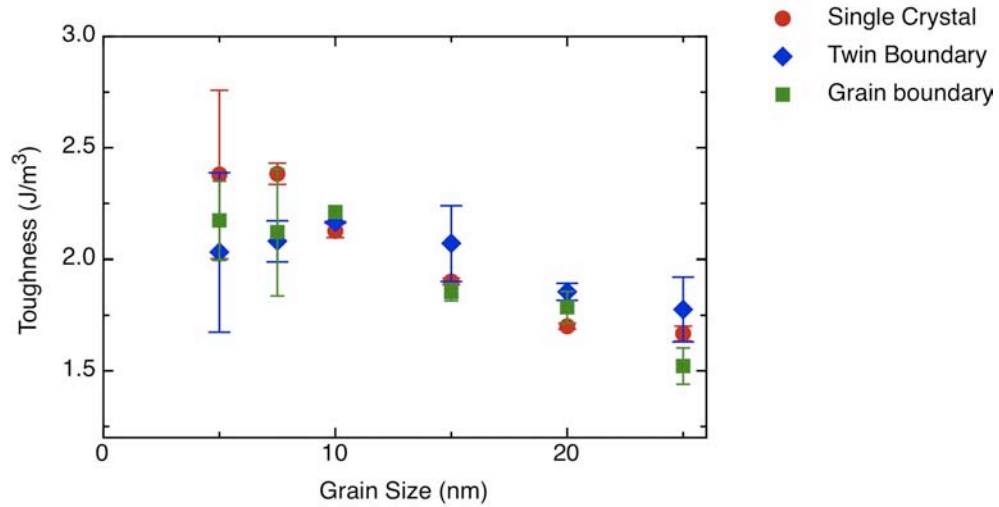
Figure 3.11 Variations in U or toughness of three simulated systems with respect to the crystal size.

It needs to indicate that as the system size decreases, the uncertainty of U obtained from simulation increases, as demonstrated by the larger data scattering. This could be attributed to the increase in the ratio of boundary zone to the crystalline zone and accompanied rise of the total internal stress. These make the situation more complicated. Further studies are needed in order to clarify unclear issues when the nano-crystal size is extremely small.

3.5 Summary

The tensile behavior of nano-twinned and nano-grained systems with respect to the crystal size in comparison with that of single crystal is studied. The results show that unlike the grain boundary that acts as a sink to attract/block dislocations and also a source to emit dislocations, the twin

boundary acts mainly as a dislocation blocker and performs more effectively than the grain boundary. The single crystal shows the largest difficulty for dislocations to form.

As the grain size is below about ~ 10 nm, inverse Hall-Petch relation occurs in the GB-containing system. The present study suggests that the inverse Hall-Petch relation does not necessarily result from grain boundary sliding. The inverse Hall-Petch relation is not applicable to nano-twinned system under the present simulation condition.

The U value increases with decreasing the crystal size; however, below 10 nm the toughness of both TB-containing and GB-containing systems decreases but this is not the case for the single crystal system. As the crystal size is below 10 nm, the uncertainty of the energy absorption capability or toughness increases, corresponding to larger data scattering.

Chapter 4 Responses of twin boundaries to two-directional sliding

In previous chapter, nano-twinned model system is proved to have a higher strength than nanocrystalline model system, which demonstrates that nano-twinned Cu could be a good candidate for dynamic electrical contacts. In dynamic systems, electrical contacts suffer from fretting, i.e., small-amplitude oscillation in the contract area. Fretting defines the situation where one contact element is subjected to a low amplitude alternative displacement with respect to the other contact element, against which it is pressed[1]. Fretting generally introduces plastic deformation and may raise interfacial temperature to certain degree, both of which increase the electrical contact resistance, resulting from enhanced electron scattering by defects such as dislocations and possible oxidation. The loss of conductivity of dynamic electrical contacts during fretting processes is always a problem that attracts long-term attention.

In this chapter, nano-twinned copper has been studied under simulated "fretting" condition. How the nano-twinning affects the increase in the local dislocation density is investigated in comparison with nano-grain boundaries under one-directional and two-directional sliding conditions.

4.1 Background

In order to solve the fretting problem, nanocrystalline Cu was expected to exhibit high fretting resistance while maintaining desired electric conductivity. However, it turned out that the electrical resistance of nanocrystalline is too high due to enhanced electron scattering by high-density grain boundaries. Recent studies demonstrate that introduction of Nano-twinning is a very promising approach[6]. Nano-twinning results in an increase in strength which is significantly higher than that caused by grain boundaries, while maintaining much lower electrical resistance, compared to grain boundaries, due to its ordered twin boundary structures[24, 27, 40, 66, 67].

During fretting, plastic deformation accumulates, corresponding to an increase in dislocation density, which elevates the electrical resistance. Increases in dislocation density in single, nano-twinned and nano-grained crystals could be very different. One of the main objectives of the present study is to investigate dislocation accumulations in the above-mentioned three copper model systems under the same loading condition, e.g., tension. This portion of work has been reported in the previous chapter.

Another issue is related to the wearing condition. It is noticed that a metal may respond to single-directional sliding and two-directional sliding (back-and-forth) differently. In the latter case, material softening may occur corresponding to a reduction of the strain-hardening rate, but this is not the

case for one-directional sliding. Bauschinger effect seems play a role during two-directional sliding wear. Bauschinger effect refers to a change in yield strength with stress reversal. For example, a plastically pre-strained metal in compression may have lower tensile yield strength. The Bauschinger effect results from reversible dislocation movement and annihilation of dislocations having opposite signs[68, 69]. Hasegawa et al [70]studied the deformation behavior of aluminum and demonstrated that dislocation cells or subgrains formed at room temperature were unstable against the stress reversal. However, the formation of unstable dislocation structures and their variations have still not been fully understood yet, largely due to the difficulty in performing relevant experiments, e.g., it is difficult to track dislocation movement. Computer simulation provides a supplementary and effective approach, which is particularly suitable for studying various phenomena at the nanoscale. Fang *et al* simulated Bauschinger effect in nickel with three different model systems, single crystal, low angle grain boundaries and high angle grain boundaries at the nanoscale[71]. The results suggested that the single crystal could have the smallest Bauschinger effect and high angle grain boundary showed the strongest Bauschinger effect.   M. Haouaoui *et al* investigated the flow stress anisotropy and Bauschinger effect in ultrafine grained copper; and noticed that the grain morphology and grain boundary character are of importance to the Bauschinger effect[72]. Studies of Bauschinger effect in twinning systems are lacking. Although some relevant studies have been reported, e.g., dislocation pileup at twin

boundaries by Haraman et al[68, 73], available information is very limited.

In this chapter, a preliminarily study is reported on how the dislocation density changes during one-directional sliding and two-directional sliding in the nano-twinned system in comparison with those in single crystal and nanocrystalline systems.

4.2 Simulation geometry

The molecular dynamics method is employed for this study on three model systems, including single crystal, bicrystal with a twin boundary (TW), and bicrystal with a grain boundary (GB) as illustrated in Figure 4.1. All three systems have the same system size of 20.1nmx9.35nmx3.5nm, consisting of about 56000 atoms. For the system of single crystal, the configuration is constructed with the crystal orientations, $[111]$, $[\bar{1}10]$ and $[11\bar{2}]$ in X-, Y- and Z- direction. For the bicrystal system with a twin boundary, the left grain has its orientations, $[111]$, $[\bar{1}10]$ and $[11\bar{2}]$, respectively parallel to the X-, Y- and Z-directions (the same as those for the single crystal). The right grain is tilted to have its orientations, $[111]$, $[1\bar{1}0]$ and $[\bar{1}\bar{1}2]$, parallel to the X-, Y- and Z-directions, forming a $\Sigma 3$ coherent twin boundary with its normal parallel to the <111> axis (in the direction along which the external force is applied) between two grains. The grain boundary bicrystal system consists of a left grain with the same orientations of that in twin boundary system and a right grain which is rotated with a angle of 38.2°. A $\Sigma 7$ twist boundary is

constructed and 1% vacancies are added to the boundary i.e., took 1% atoms from the boundary area. A rigid indenter having a semi-spherical tip with radius of 5nm using copper atomic structure is placed at the center of top surface of the left grain or ¼ system length for single crystal. The atomic interactions are described using the Mishin[55] form of the Embedded Atom Method[53] potential for copper. Lammps[63] is the software used for this simulation study.
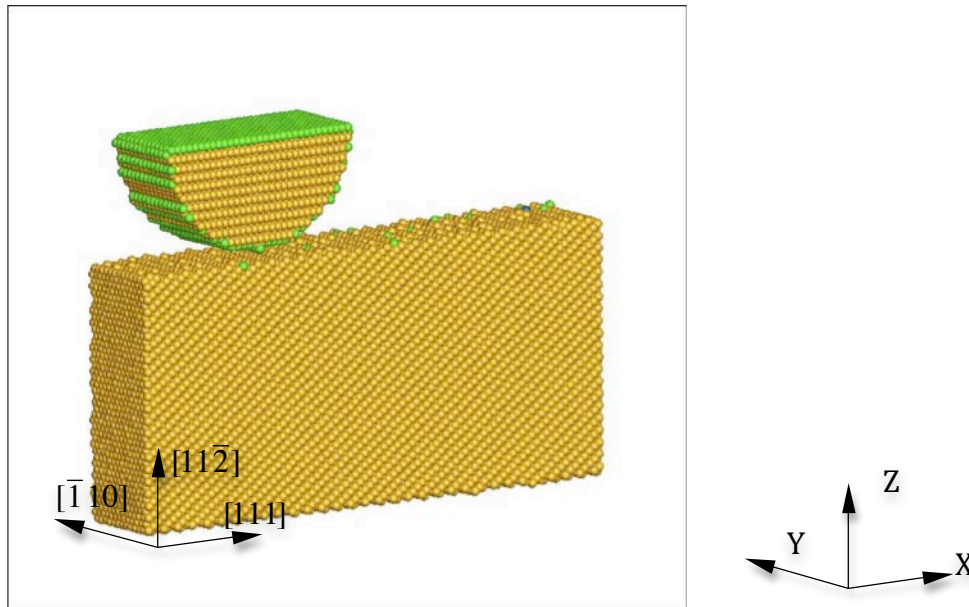
(a)
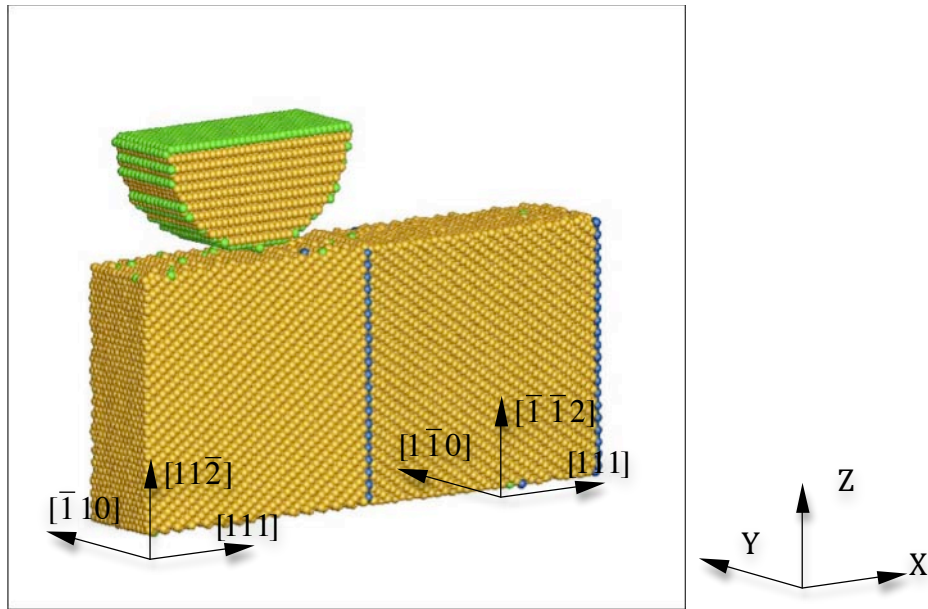
(b)
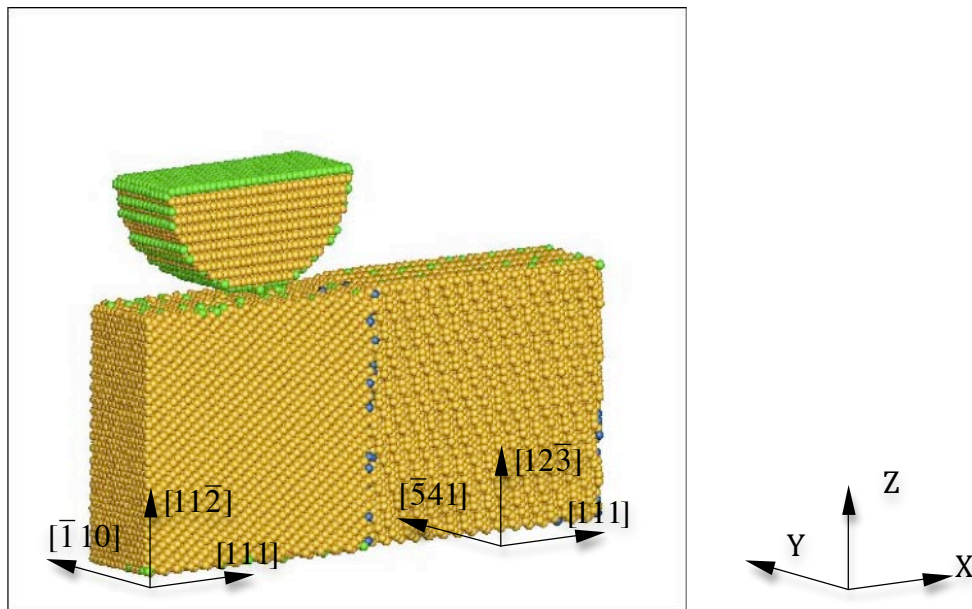
(c)

Figure 4.1 Three model systems: (a) Single crystal model system with crystal orientation $[111], [\bar{1}10]$ *and* $[11\bar{2}]$ *in the X-, Y- and Z- directions (b) Twin boundary model system. The left grain has orientations* $[111]$, $[\bar{1}10]$ *and* $[11\bar{2}]$ *in the X-, Y- and Z-directions. The right grain is tilted to the orientations*

of $[111]$,$[1\bar{1}0]$ and $[\bar{1}\,\bar{1}2]$. (c) Grain boundary model system. The left grain has orientations $[111]$, $[\bar{1}10]$ and $[11\bar{2}]$ in the X-, Y- and Z-directions. The right grain is twisted to the orientations of $[111]$, $[\bar{5}41]$ and $[12\bar{3}]$. 1% vacancies are added to the boundary region. A rigid indenter tip with its radius of 5nm as shown in the figure was used to investigate the response of the system to sliding wear. The tip has copper's lattice structure but was set as a rigid tip.

4.3 System relaxation

After the initial construction, all systems need to be relaxed before performing simulated sliding processes. The single crystal and nano-twinned model systems are thermally equilibrated to 300K for 500ps, shown in Figure 4.2 (a)(b). Relaxation is run within a NVT ensemble. Temperature is controlled using velocity-rescaling method. For grain boundary system, when constructing the initial structure, vacancies have been taken from boundary area. In order to have the GB model system closer to the reality, the initially constructed system is first heated up to 900K for 100ps, and then gradually cooled down to the room temperature (300K), see Figure 4.2(c). The system reached local minimum energy state using energy minimization method, which has been introduced in chapter2. Periodical boundary condition is utilized in the X-, Y- directions for all simulations, while free surface condition in Z- direction.
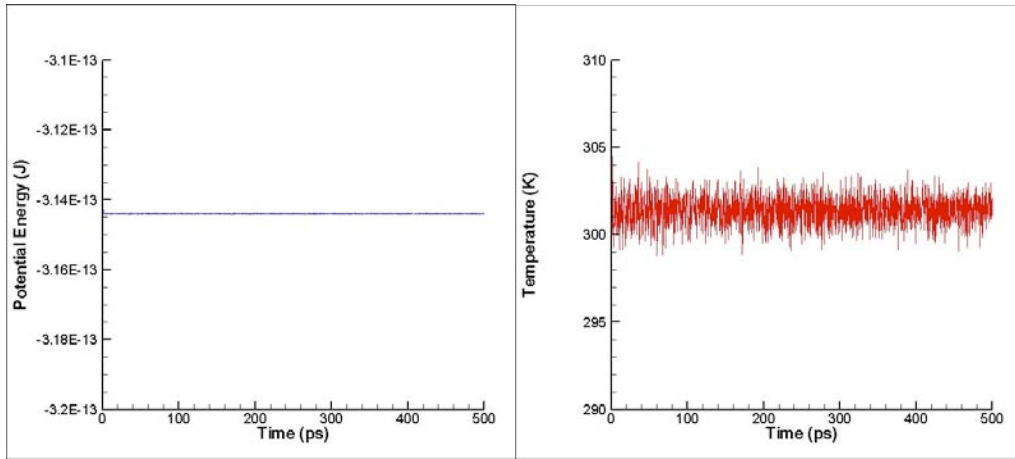
(a)
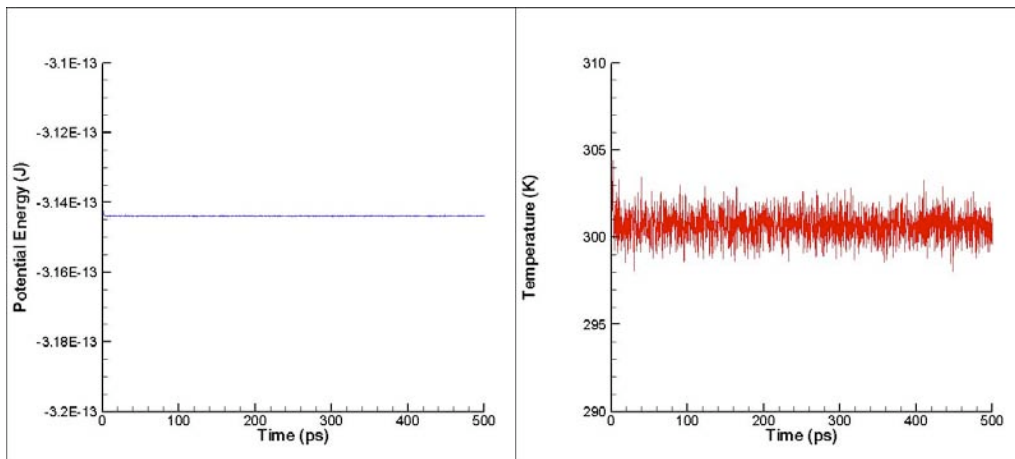
(b)
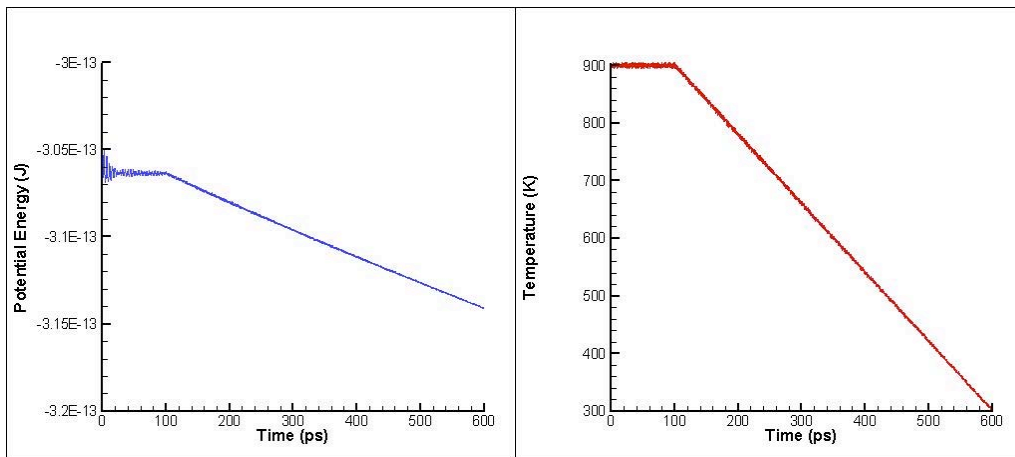
(c)

Figure 4.2 Relaxing energy and temperature of (a) single crystal model system (b) twin boundary model system (c) grain boundary model system

4.4 One-directional and two-directional sliding

The relaxed models are then simulated under two different sliding conditions: one-directional and two-directional sliding. Each sliding test contained two sliding passes. For the one-directional sliding, the indenter first moves at a speed of 0.5m/s down along Z direction until reaching a depth of 0.1nm, and then slides along X direction (parallel to <111> crystallographic direction) at the same speed until reaching the center of the right grain. This process is repeated with another 0.1 nm depth starting at the initial starting position to complete the second pass. For the two-directional sliding, the first sliding pass is the same as that of the one-directional sliding. After the first pass, the indenter moves down with a depth of 0.1 nm, and then slides back to the initial starting position. The entire process is proceeded at a constant temperature of 300K using velocity rescaling thermostat.

4.5 Results and discussion

During sliding, dislocations are generated, which interact with the twin and grain boundary and themselves. We have determined the distributions of atoms in defected zones and corresponding principle stress σ_1 (GPa) in the three different model systems shown in Figure 4.2. Figure 4.2 (a) and (b)

illustrate the situations of one-directional sliding and two-directional sliding, respectively. In the first case, more dislocations are generated in the single crystal system. Since there is no boundary, dislocations are distributed more evenly in the whole system. According to the σ_1 map, single crystal appears to have a relatively lower stress concentration. While in both the nano-twinned and nano-grained systems, dislocations are accumulated more in the left-hand side and blocked by the boundaries. Higher-tension stress exists along twin and grain boundary at right side. Under the two-directional sliding condition, the situation is similar, i.e., the single crystal system has the higher dislocation density than the boundary-containing systems. Besides, the defect density appeared to be lower during the two-directional sliding, which corresponds to Bauschinger effect.
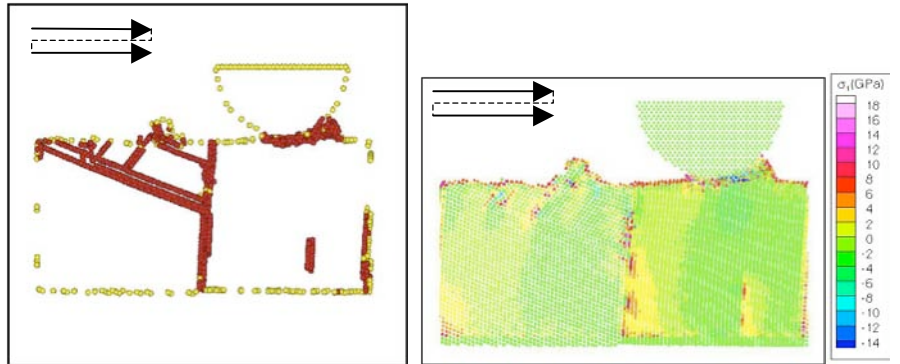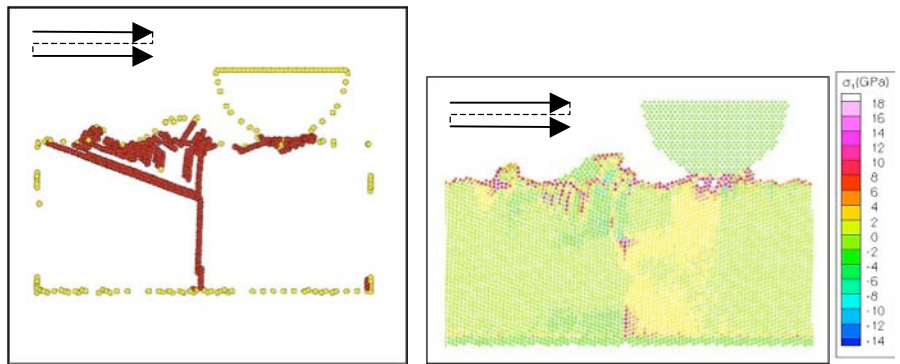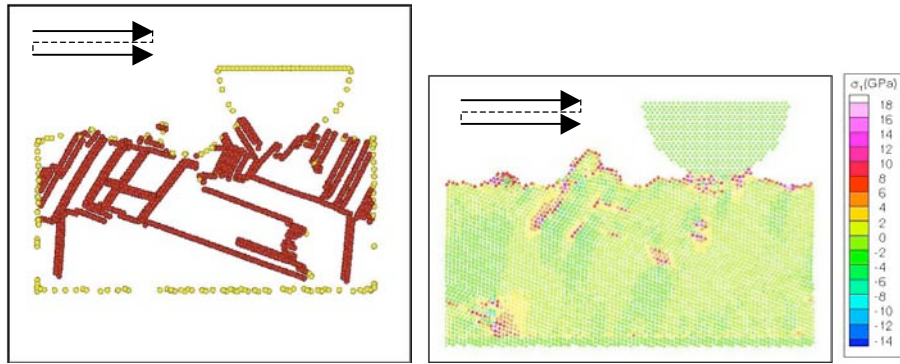
(a)
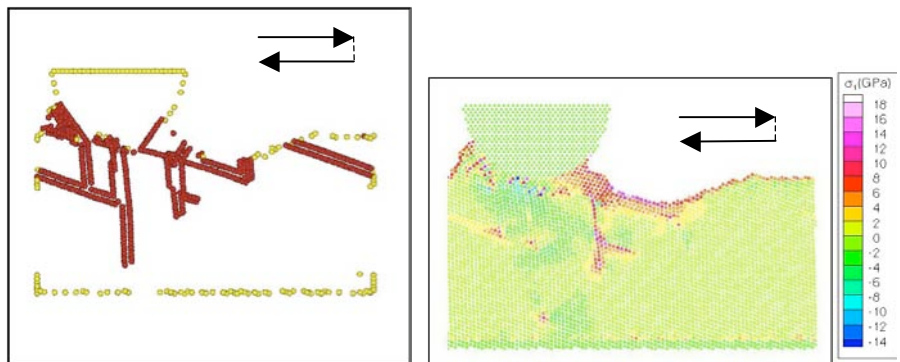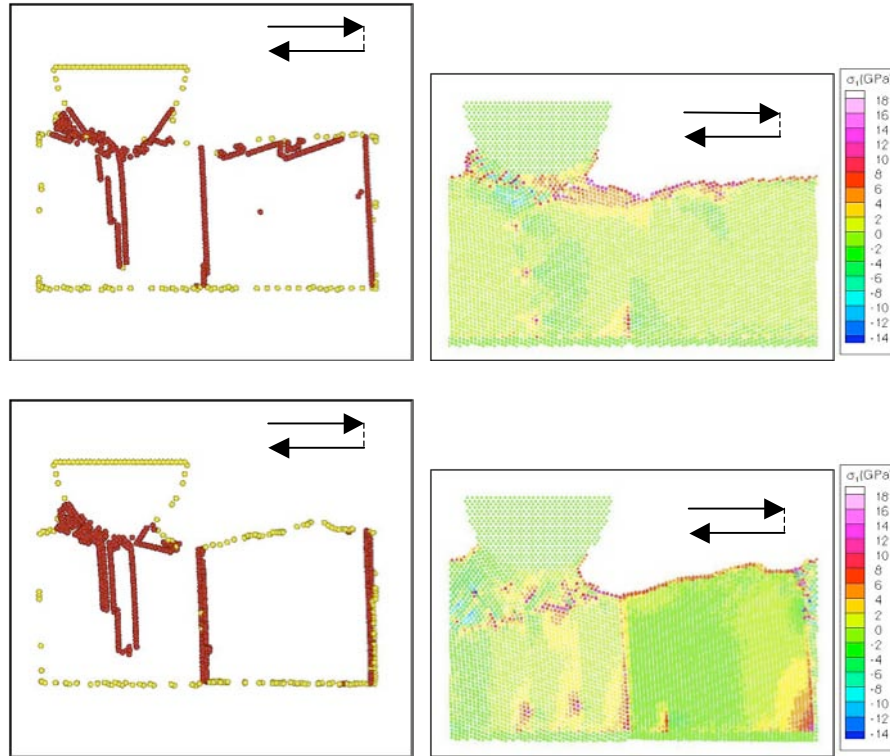
(b)

Figure 4.2 Distributions of defect and corresponding principle stress σ_1 of different model systems; single crystal, nano-twinned and nano-grained systems are illustrated (from top to bottom). (a) Three systems under single-directional sliding condition, and (b) Three systems under two-directional sliding condition. Figures in the left column show distributions of defects. Atoms in defected regions are shown in color, while defect-free regions are blank. Figures in the right column show distributions of maximum principal stress σ_1 in three model systems, respectively.

In order to further examine the Bauschinger effect, a statistical analysis is

performed by counting the atoms that belonged to defected regions as illustrated in Figure 4.2. Results of the counting are presented in Figure 4.3. As shown, in the single crystal and nano-twinned systems, the defect density decreases during two-directional sliding, suggesting the annihilation of dislocations. During the first pass, dislocations are generated inside the entire single crystal. While in nano-twinned systems, and dislocations are more accumulated in the left crystal, since they are blocked by the twin boundary. The second pass in reversed sliding direction results in reversible dislocation movement and those with opposite signs may cancel each other, leading to the decrease in dislocation density[68, 69, 74]. However, the situation of nano-grained system is different. As shown in Figure 4.3, the density of dislocations in the nano-grained system corresponding to the two-directional sliding is higher than that corresponding to the one-directional sliding. A possible explanation for such a reversed trend in the nanocrystalline system under study is that dislocation back-sliding could be easier without too much interruption by emitted dislocations from the boundary because of larger difficulty of dislocation emission from twin boundaries; while the situation could be reversed for the grain boundary that plays a dual role as a sink and also a source for dislocations [75, 76], since (1) dislocation emission is easier from grain boundaries[11, 77] and (2) the emitted and previous ones may interact. These factors may be responsible for the increase in dislocation density during two-directional sliding for the GB-containing system. The result of simulation implies that nano-twinned Cu

would possess higher resistance to defect accumulation caused by fretting than nanocrystalline Cu, so that the former has a stronger capability to maintain its conductivity. The simulation, though only for simple model systems, lead to an insight into the mechanism for the experimental observation[6]. Besides, the simulation suggests that high-density grain boundaries in a nanocrystalline metal could make the material behave differently from its microcrystalline counterpart in terms of Bauschinger effect.
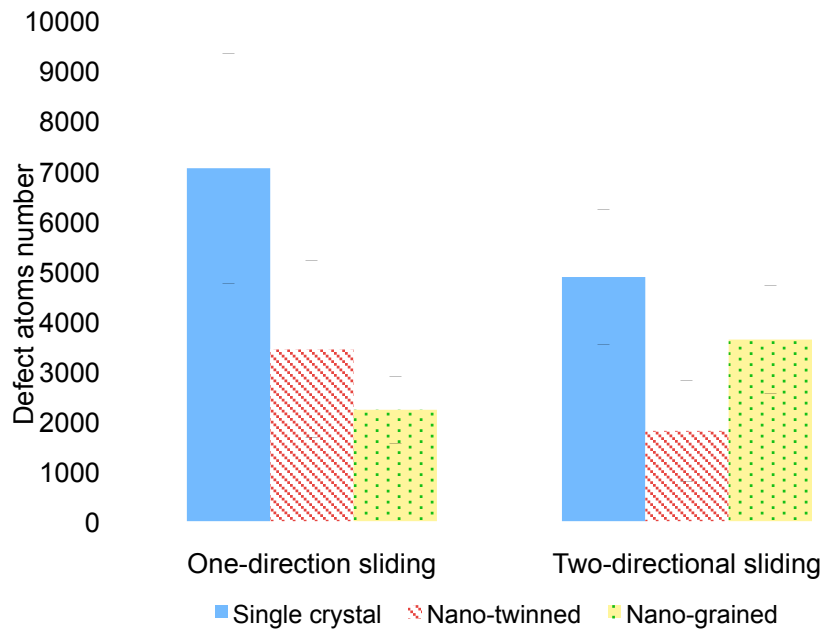
Figure 4.3 Densities of defect in single crystal, twin boundary and grain boundary model systems, generated during one-directional and two-directional sliding processes.

4.6 Summary

The modeling study demonstrates that dislocations are easier to be generated in the single crystal system than those in the nano-twinned and nano-grained systems. The increase in dislocation density is marked lower in the nano-twinned system than in the nano-grained system. During two-directional or forth-and-back sliding process, Bauschinger effect is observed in the single crystal and nano-twinned systems, corresponding to decreases in dislocation density. However, the situation is opposite for the nano-grained system. The nano-twinned Cu shows the least dislocation accumulation during two-directional sliding under the present simulation condition. Thus, both high resistance to fretting and low electrical resistance can be anticipated to obtain from nano-twinned copper.

Chapter 5 Conclusions and future work

5.1 General conclusions

In this thesis study, nano-twinned Cu is studied through the molecular dynamics simulation with tasks of studying the mechanical behavior and preliminary investigating defect generation during one-directional and two-directional sliding processes. In addition to a nano-twinned system, single crystal and nanocrystalline Cu model systems have also been studied for comparison purpose. Responses of three systems to stress at nano scales are studied. Responses of the systems to one-directional and two-directional sliding processes are also investigated to see how the nano-twinning affects the increase in the local dislocation density in comparison with nano-grain boundaries under one-directional and two directional sliding conditions. The following are main conclusions drawn from this study:

1) Three model systems with grain sizes in the critical range of 5nm ~ 25nm are studied. Under tensile stress, the grain boundary behaves as a sink and also a source to attract and emit dislocations. Compared to the grain boundary, a nano-twinned boundary acts mainly as the obstacle of dislocations and performs more effectively in strengthening the metal. The results also show that it is the most difficult to form dislocations in the single

crystal.

2) Inverse Hall-Petch relation is observed in the systems with the nano-GBs when the grain size is below about 10nm. With uniaxial loading and fixed boundary condition, the simulation results suggests that the inverse Hall-Petch relation does not necessarily result from grain boundary sliding. Enhanced dislocation emission could also contribute to the inverse Hall-Petch relation. The inverse Hall-Petch relation is not applicable to nano-twinned system under the present simulation condition.

3) The toughness increases with decreasing the crystal size in all three model systems. However, when grain size is below 10 nm, the toughness of both TB-containing and GB-containing systems decreases but this is not the case for the single crystal system. As the crystal size is below 10 nm, the uncertainty of the energy absorption capability or toughness increases, corresponding to larger data scattering.

4) The modeling study shows that more dislocations are introduced in the single crystal system than in the nano-twinned and nano-grained systems. During the two-directional or forth-and-back sliding process, Bauschinger effect is observed in

the single crystal and nano-twinned systems (showing a decrease in dislocation density) during two-directional sliding in comparison with one directional sliding, while the situation is opposite for the nano-grained system. The nano-twinned Cu shows the least dislocation accumulation during two-directional sliding which should correspond to the least increase in the electrical resistance caused by fretting.

5.2 Suggested follow-up studies

As a candidate of electrical contacts, besides super mechanical properties, low electrical resistivity is required. Experiments reported in the literature show that nano-twinned copper has a considerably higher electrical conductivity than nanocrystalline copper[6, 36]. Theoretical analysis regarding how a nano-twinned boundary structure affects the electrical resistivity is still lacking and should be studied in future.

Beside, how the electrical resistivity of nano-twinned boundary varies when plastic deformation occurs is unclear. In-depth studies on the electrical behavior of nano-twinning when plastic deformation is involved, e.g., during tensile test or wear process could be an interesting topic for future work.

In present study, all simulations are performed for simply structured models such as the bicrystal or three grains system in order to focus on local events of the material. The simulation data when grain size is below 10nm is

scattered and thus not as reliable as that of larger grain size in tensile test, due to the uncertainty of the energy absorption capability. In this case, polycrystalline structured model systems containing more boundaries (grain boundaries or twin boundaries) are suggested to repeat the simulation tests. Such systems with more boundaries may be better represent realistic nanostructured materials with possible minimization of the uncertainty problem.

In sliding test, defect density result data showed large fluctuations in all simulation models. The defect density was calculated based on the final snapshot of sliding processes. In the simulation, the top surface is free surface, from which partial dislocations could generate or slip off. This increases the uncertainty of counting the atoms number from defect regions. In addition, the regions with defects are identified using order parameter method introduced in chapter 2, which marks all the atoms that not belongs to FCC structure. However the random structured accumulation at contact area will have a remarkable influence on defect density result. Recently, a quantitative analysis of plasticity[78] is developed separating the contributions from partial dislocations perfect dislocations multiple dislocations. Bringing in such method, an "in-situ" observation of dislocations movement and density changing though the whole sliding process could be performed in future.

Finally, due to the time issue the currently simulated two-directional sliding process only includes two passes, which does not well represent a

fretting process. Multiple-pass sliding processes should be simulated in future in order to bring the simulation closer to realistic simulations.

Bibliography

[1] Hannel S, Fouvry S, Kapsa P, Vincent L. Wear 2001;249:761.

[2] Malucci RD, Ieee. Impact of fretting parameters on contact degradation. Electrical Contacts - 1996: Proceedings of the Forty-Second Ieee Holm Conference on Electrical Contacts - Joint with the 18th International Conference on Electrical Contacts. 1996. p.395.

[3] Wang YM, Chen MW, Zhou FH, Ma E. Nature 2002;419:912.

[4] Mayadas AF, Shatzkes M. Phys Rev B 1970;1:1382.

[5] Sun T, Yao B, Warren AP, Barmak K, Toney MF, Peale RE, Coffey KR. Phys Rev B 2009;79.

[6] Lu L, Shen YF, Chen XH, Qian LH, Lu K. Science 2004;304:422.

[7] Van Swygenhoven H, Derlet PM, Hasnaoui A. Phys Rev B 2002;66.

[8] de Koning M, Miller R, Bulatov VV, Abraham FF. Philos Mag A 2002;82:2511.

[9] Dao M, Lu L, Asaro RJ, De Hosson JTM, Ma E. Acta Mater 2007;55:4041.

[10]   Zhu T, Li J, Samanta A, Kim HG, Suresh S. P Natl Acad Sci USA 2007;104:3031.

[11]   Schiotz J, Jacobsen KW. Science 2003;301:1357.

[12]   Nam HS, Srolovitz DJ. Phys Rev Lett 2007;99:025501.

[13]   Li DY, Chen Q, Wang XY. J Appl Phys 2006;99:044305.

[14]   Zhang HY, Hu ZQ, Lu K. J Appl Phys 1995;77:2811.

[15]   Anderoglu O, Misra A, Wang H, Ronning F, Hundley MF, Zhang X. Appl Phys Lett 2008;93:083108.

[16]   Van Swygenhoven H, Spaczer M, Caro A. Acta Mater 1999;47:3117.

[17]   Conrad H, Narayan J. Scripta Mater 2000;42:1025.

[18]   Krasilnikov N, Lojkowski W, Pakiela Z, Valiev R. Mater. Sci. Eng. A-Struct. Mater. Prop. Microstruct. Process. 2005;397:330.

[19]   Hosford WF. Mechanical behavior of materials. Cambridge ; New York: Cambridge University Press.

[20]   Chen MW, McCauley JW, Dandekar DP, Bourne NK. Nat Mater 2006;5:614.

[21]   Blewitt TH, Coltman RR, Redman JK. J Appl Phys 1957;28:651.

[22]   Nolder RL, Thomas G. Acta Metall Mater 1964;12:227.

[23]   Johari O, Thomas G. Acta Metall Mater 1964;12:1153.

[24]   Yamakov V, Wolf D, Phillpot SR, Gleiter H. Acta Mater 2002;50:5005.

[25]   Chen MW, Ma E, Hemker KJ, Sheng HW, Wang YM, Cheng XM. Science 2003;300:1275.

[26]   Sanders PG, Eastman JA, Weertman JR. Acta Mater 1997;45:4019.

[27]   Ma E, Wang YM, Lu QH, Sui ML, Lu L, Lu K. Appl Phys Lett 2004;85:4932.

[28]   Lu L, Chen X, Huang X, Lu K. Science 2009;323:607.

[29]   Hall EO. Proceedings of the Physical Society of London Section B 1951;64:747.

[30]   Petch NJ. Journal of the Iron and Steel Institute 1953;174:25.

[31]   Schiotz J, Di Tolla FD, Jacobsen KW. Nature 1998;391:561.

[32]   Van Swygenhoven H, Spaczer M, Caro A, Farkas D. Physical Review B 1999;60:22.

[33]   Yip S. Nature 1998;391:532.

[34]   Schiotz J, Vegge T, Di Tolla FD, Jacobsen KW. Physical Review B 1999;60:11971.

[35]   Yamakov V, Wolf D, Phillpot SR, Mukherjee AK, Gleiter H. Nat Mater 2002;1:45.

[36]   Qian LH, Lu QH, Kong WJ, Lu K. Scripta Mater 2004;50:1407.

[37]   Andrews PV, West MB, Robeson CR. Philos Mag 1969;19:887.

[38]   Schwarz H, Luck R. Mater Sci Eng 1970;5:149.

[39]   Cao A, Wei YG, Ma E. Physical Review B 2008;77:195429.

[40]   Cao AJ, Wei YG, Mao SX. Appl Phys Lett 2007;90:151909.

[41]   Cao AJ, Wei YG. J Appl Phys 2007;102:083511.

[42]   Li L, Ghoniem NM. Phys Rev B 2009;79.

[43]   Spearot DE, Tschopp MA, Jacob KI, McDowell DL. Acta Mater 2007;55:705.

[44]   Tschopp MA, Tucker GJ, McDowell DL. Comp Mater Sci 2008;44:351.

[45]   Shabib I, Miller RE. Model Simul Mater Sc 2009;17:055009.

[46]   Haile JM, Mansoori GA, American Chemical Society. Division of Industrial and Engineering Chemistry., American Chemical Society. Division of Physical Chemistry., American Chemical Society. Meeting. Molecular-based study of fluids. Washington, D.C.: American Chemical Society, 1983.

[47]   Alder BJ, Wainwright TE. J Chem Phys 1957;27:1208.

[48]   Allen MP, Tildesley DJ. Computer simulation of liquids. Oxford [England]

New York: Clarendon Press ;

Oxford University Press, 1987.

[49]   Haile JM. Molecular dynamics simulation : elementary methods. New York: Wiley, 1992.

[50]   Verlet L. Phys Rev 1967;159:98.

[51]   Swope WC, Andersen HC, Berens PH, Wilson KR. J Chem Phys 1982;76:637.

[52]   Jones JE. P R Soc Lond a-Conta 1924;106:463.

[53]   Foiles SM, Baskes MI, Daw MS. Phys Rev B 1986;33:7983.

[54]   Daw MS, Baskes MI. Phys Rev B 1984;29:6443.

[55]   Mishin Y, Mehl MJ, Papaconstantopoulos DA, Voter AF, Kress JD. Phys Rev B 2001;6322:224106.

[56]   Nosé S. J Chem Phys 1984;81:511.

[57]   Hoover W, Holian B. Physical Review a-General Physics 1996;211:253.

[58]   Parrinello M, Rahman A. Phys Rev Lett 1980;45:1196.

[59]   Parrinello M, Rahman A. J Appl Phys 1981;52:7182.

[60]   Steinhardt PJ, Nelson DR, Ronchetti M. Phys Rev B 1983;28:784.

[61]   Vanduijneveldt JS, Frenkel D. J Chem Phys 1992;96:4655.

[62]   Chushak Y, Bartell LS. J Phys Chem A 2000;104:9328.

[63]   Plimpton S. J Comput Phys 1995;117:1.

[64]   Schuh CA, Nieh TG, Yamasaki T. Scripta Mater 2002;46:735.

[65]   Hall EO. P Phys Soc Lond B 1951;64:742.

[66]   Zhang YS, Han Z, Wang K, Lu K. Wear 2006;260:942.

[67]   Zhang YS, Wang K, Han Z, Liu G. Wear 2007;262:1463.

[68]   Pedersen OB, Brown LM, Stobbs WM. Acta Metall Mater 1981;29:1843.

[69]   Kuwabara T, Kumano Y, Ziegelheim J, Kurosaki I. Int J Plasticity 2009;25:1759.

[70]   Hasegawa T, Yakou T, Karashima S. Mater Sci Eng 1975;20:267.

[71]   Fang H, Horstemeyer MF, Baskes MI, Solanki K. Comput Method Appl M 2004;193:1789.

[72]   Haouaoui M, Karaman I, Maier HJ. Acta Mater 2006;54:5477.

[73]   Karaman I, Sehitoglu H, Chumlyakov YI, Maier HJ, Kireeva IV. Metall Mater Trans A 2001;32:695.

[74]   Bate PS, Wilson DV. Acta Metall Mater 1986;34:1097.

[75]   Van Swygenhoven H, Derlet PM, Hasnaoui A. Phys Rev B 2002;66.

[76]   Yue L, Zhang H, Li DY. Acta Mater 2010;58:2677.

[77]   Meyers MA, Mishra A, Benson DJ. Prog Mater Sci 2006;51:427.

[78]   Vo NQ, Averback RS, Bellon P, Odunuga S, Caro A. Phys Rev B 2008;77.